Cell and Tissue Research (2024) 396:119–139
https://doi.org/10.1007/s00441-024-03868-9

REGULAR ARTICLE

Comparative transcriptomic and phenotypic analysis of induced pluripotent stem cell hepatocyte-like cells and primary human hepatocytes

Neeti Gandhi[1] · Lauren Wills[2] · Kyle Akers[3] · Yiqi Su[4] · Parker Niccum[3] · T. M. Murali[4] · Padmavathy Rajagopalan[1,2]

Received: 13 February 2023 / Accepted: 22 January 2024 / Published online: 19 February 2024

Abstract

Primary human hepatocytes (PHHs) are used extensively for in vitro liver cultures to study hepatic functions. However, limited availability and invasive retrieval prevent their widespread use. Induced pluripotent stem cells exhibit significant potential since they can be obtained non-invasively and differentiated into hepatic lineages, such as hepatocyte-like cells (iHLCs). However, there are concerns about their fetal phenotypic characteristics and their hepatic functions compared to PHHs in culture. Therefore, we performed an RNA-sequencing (RNA-seq) analysis to understand pathways that are either up- or downregulated in each cell type. Analysis of the RNA-seq data showed an upregulation in the bile secretion pathway where genes such as AQP9 and UGT1A1 were higher expressed in PHHs compared to iHLCs by 455- and 15-fold, respectively. Upon immunostaining, bile canaliculi were shown to be present in PHHs. The TCA cycle in PHHs was upregulated compared to iHLCs. Cellular analysis showed a 2–2.5-fold increase in normalized urea production in PHHs compared to iHLCs. In addition, drug metabolism pathways, including cytochrome P450 (CYP450) and UDP-glucuronosyltransferase enzymes, were upregulated in PHHs compared to iHLCs. Of note, CYP2E1 gene expression was significantly higher (21,810-fold) in PHHs. Acetaminophen and ethanol were administered to PHH and iHLC cultures to investigate differences in biotransformation. CYP450 activity of baseline and toxicant-treated samples was significantly higher in PHHs compared to iHLCs. Our analysis revealed that iHLCs have substantial differences from PHHs in critical hepatic functions. These results have highlighted the differences in gene expression and hepatic functions between PHHs and iHLCs to motivate future investigation.

Keywords Human induced pluripotent stem cells · Hepatocytes · In vitro liver · RNA-seq · Gene expression

Introduction

Since their discovery, induced pluripotent stem cells (iPSCs) have gained attention for their potential in various applications for in vitro and in vivo applications, such as organoids, toxicity and drug studies, disease modeling, and regenerative medicine (Mora et al. 2017; Rowe and Daley 2019; Shi et al. 2017). iPSCs were discovered in 2006 by Takahashi and Yamanaka (2006). Since then, iPSCs have been differentiated into neural, intestinal, liver, retinal, cardiac, and muscle cells (Wills and Rajagopalan 2020). Various protocols have been reported to differentiate iPSCs into hepatocyte-like cells (iHLCs) (Kaserman and Wilson 2017; Krumm et al. 2022; Mallanna and Duncan 2013; Sauer et al. 2014; Si-Tayeb et al. 2010; Song et al. 2009; Takebe et al. 2013; Xu et al. 2018). The differentiation protocols for iHLCs are based on procedures used to obtain hepatocytes from embryonic stem cells (ESCs) (Kaserman and Wilson 2017; Krumm et al. 2022; Mallanna and Duncan 2013; Sauer et al. 2014; Si-Tayeb et al. 2010; Takebe et al. 2013; Wills and Rajagopalan 2020). The first step is to obtain the definitive endoderm through the addition of Activin A and Wnt3a (Krumm et al. 2022; Mallanna and Duncan 2013; Sauer et al. 2014; Si-Tayeb et al. 2010; Takebe et al. 2013). Thereafter, cells are targeted toward hepatoblasts, or immature hepatocytes, through the addition of bone morphogenetic factor-4 (BMP-4) and fibroblast

✉ Padmavathy Rajagopalan
padmar@vt.edu

1 Department of Chemical Engineering, Virginia Tech, 333 Kelly Hall, Blacksburg, VA 24061, USA

2 School of Biomedical Engineering and Sciences, Virginia Tech, Blacksburg, USA

3 Genetics, Bioinformatics, and Computational Biology Ph.D. Program, Virginia Tech, Blacksburg, VA, USA

4 Department of Computer Science, Virginia Tech, Blacksburg, VA, USA

growth factor-2 (FGF-2) (Krumm et al. 2022; Mallanna and Duncan 2013; Sauer et al. 2014; Si-Tayeb et al. 2010; Song et al. 2009; Takebe et al. 2013). The hepatoblasts are further matured to hepatocytes by adding hepatocyte growth factor (HGF) followed by a mixture of oncostatin M and dexamethasone (Kaserman and Wilson 2017; Krumm et al. 2022; Mallanna and Duncan 2013; Sauer et al. 2014; Si-Tayeb et al. 2010; Takebe et al. 2013; Xu et al. 2018). Each of these steps leads to the development, maturation, and functionality of hepatocytes (Kaserman and Wilson 2017; Krumm et al. 2022; Mallanna and Duncan 2013; Sauer et al. 2014; Si-Tayeb et al. 2010; Song et al. 2009; Takebe et al. 2013; Xu et al. 2018). Other molecules used for differentiation of iPSCs to iHLCs include VEGF, EGF, TGF-α, and vitamin K (Kaserman and Wilson 2017; Xie et al. 2021). Adding chemical cocktails is the most common method for the maturation and differentiation of iHLCs (Kaserman and Wilson 2017; Krumm et al. 2022; Mallanna and Duncan 2013; Sauer et al. 2014; Si-Tayeb et al. 2010; Song et al. 2009; Takebe et al. 2013; Xu et al. 2018). Other methods can include the addition of small molecules (DMSO, valproic acid), different culture systems (spheroids, scaffolds, organoids), and genetic reprogramming (transcription factors and miRNAs) (Du et al. 2018; Laudadio et al. 2012; Lauschke et al. 2016; Wang et al. 2016; Xie et al. 2021). The generation of iHLCs is typically confirmed by albumin expression, accumulation of glycogen, urea synthesis, lipid metabolism, and expression of cytochrome P450 (CYP450) enzymes (Kaserman and Wilson 2017; Krumm et al. 2022; Mallanna and Duncan 2013; Sauer et al. 2014; Si-Tayeb et al. 2010; Song et al. 2009; Takebe et al. 2013; Xu et al. 2018). However, studies have reported that iHLCs exhibit lower expression of enzymes involved in metabolism and biotransformation (Si-Tayeb et al. 2010; Song et al. 2009; Xu et al. 2018).

Traditionally, primary human hepatocytes (PHHs) are considered to be the most relevant for in vitro liver investigations (Godoy et al. 2013; Wills and Rajagopalan 2020). However, disadvantages of these cells include invasive retrieval, significant donor variability, and limited availability (Godoy et al. 2013; Wills and Rajagopalan 2020; Zeilinger et al. 2016).

Genome-wide transcriptomic analyses have been conducted to investigate the similarities and differences between iHLCs and either the liver in vivo, PHHs, or hepatic cell lines (Gao and Liu 2017; Gupta et al. 2021; Sjogren et al. 2014; Viiri et al. 2019). We first focused on reports that have shown similar characteristics between iHLCs and mature hepatic cells (Gao and Liu 2017; Gupta et al. 2021; Sjogren et al. 2014; Viiri et al. 2019). Sjogren et. al. reported that iHLCs were more similar to PHHs than Huh7 and HepRG cells. Their results indicated a lower number of differentially expressed genes involved in nine apoptotic pathways (genes not reported) (Sjogren et al. 2014). Another comprehensive gene expression analysis study compared iHLCs to PHHs from six donors, as well as several cell lines including HepRG, Huh7, HepG2, and HepG2/C3A (Gao and Liu 2017). The results indicated that iHLCs were more closely related to PHHs compared to the hepatoma cell lines, except HepRG, in drug metabolizing pathways, as determined by principal component analyses (PCA) (Gao and Liu 2017). While iHLCs have been shown to exhibit phenotypic characteristics that emulate mature hepatic cells, significant differences have also been revealed. The same study also showed that CYP3A7, an enzyme expressed in fetal livers, had a higher relative gene expression in iHLCs (11.9–13.4) compared to PHHs (8.5) (Gao and Liu 2017). A qPCR analysis of drug metabolizing pathways also showed that the expression levels of CYP2E1 and CYP3A4, two members of the CYP450 enzyme family, in iHLCs were 0.2% and 0.7%, respectively, of the PHH values (Sjogren et al. 2014). A transcriptomic analysis using RNA-sequencing (RNA-seq) also compared iHLCs from two commonly used differentiation protocols and PHHs (Viiri et al. 2019). This study focused on long non-coding RNAs and transcription factors involved in the differentiation pathways of iPSCs to iHLCs (Viiri et al. 2019). Results showed that transcriptional regulators such as RARG, E2F1, and FOXH1, which are involved in hepatocyte maturation, were downregulated in iHLCs compared to PHHs, which could contribute to their immaturity (Viiri et al. 2019).

To further understand the variations between PHHs and iHLCs, we measured gene expression levels in each cell type using RNA-seq data. We computed genes that were differentially expressed between the two types of cells (Wang et al. 2009). Then, we investigated pathways that were upregulated in PHHs compared to iHLCs as revealed by analysis of RNA-seq data. We focused on specific genes involved in pathways that contribute to differences between iHLCs and PHHs, such as drug metabolism, hepatocyte phenotype, bile secretion, and the citric acid cycle. To support the 'omic data, we have validated the differences in gene expression with cellular analysis. By understanding the transcriptomic differences between iHLCs and PHHs, we provide a basis for reports of experimentally observed differences in their functional capabilities.

Materials and methods

RPMI 1640, B-27 supplement, phosphate buffered saline (PBS), Tris–HCl, ethylenediaminetetraacetic acid (EDTA), ethanol (EtOH), bovine serum albumin (BSA), and TrypLE were obtained from Thermo Fisher Scientific (Waltham, MA). Gentamicin, collagenase, β-mercaptoethanol, Tris, sodium dodecyl sulfate (SDS), 7-methoxy-4-trifluoromethylcoumarin (MFC), 7-hydroxy-4-trifluoromethylcoumarin (HFC),

β-glucuronidase/arylsulfatase, and acetaminophen (APAP) were purchased from Millipore Sigma (St. Louis, MO). Oncostatin M was obtained from R&D Systems (Minneapolis, MN). Dexamethasone was purchased from MP Biomedicals (Solon, OH).

Extraction of type 1 collagen

Collagen was extracted from rat tails as described in previous reports (Larkin et al. 2013; Orbach et al. 2017). Briefly, tendons obtained from rat tails were dissolved in acetic acid and were purified through centrifugation at 13,000 × *g*. Collagen was precipitated with 30% (w/v) sodium chloride and then dialyzed in 1 mM hydrochloric acid. The solution was sterilized with chloroform and maintained at a concentration of 2.0–3.0 mg/mL at a pH of 3.1. Each well of a 6-well tissue culture polystyrene (TCPS) plate was coated with 0.5 mL of 1.1 mg/mL collagen and allowed to gel for approximately 45 min at 37 °C.

Culturing iHLCs and PHHs

iHLCs (iCell Hepatocytes 2.0) were purchased from Fujifilm (Santa Ana, CA). Cells were seeded at a density of 300,000 cells/cm^2 on collagen gels (1.1 mg/mL) and cultured according to the manufacturer's protocol. Culture medium was changed every 24 h. Plating media consisted of RPMI supplemented with Oncostatin M (10 µg/mL), dexamethasone (5 mM), gentamicin (50 mg/mL), B-27 supplement (2% v/v), and iCell Hepatocytes 2.0 medium supplement. Cells were maintained in maintenance media, containing RPMI, dexamethasone (5 mM), gentamicin (50 mg/mL), B-27 supplement (2% v/v), and iCell Hepatocytes 2.0 medium supplement, 5 days after seeding. iHLC monocultures were maintained for up to 7 days prior to conducting liver-specific testing. To assemble the collagen sandwich (CS), a second layer of collagen (1.1 mg/mL) was added 7 days after iHLC seeding (Fig. 1a). Spent culture medium was collected every 24 h and stored at −80 °C until analyzed. Cells were maintained at 37 °C in a humidified environment at 5% carbon dioxide.

PHHs were obtained from Sekisui XenoTech (Kansas City, KS). PHHs were cultured and maintained according to the manufacturer's protocol. PHHs were initially seeded on collagen gels (1.1 mg/mL) at a density of 560,000 cells/well for 6-well TCPS plates and 35,000 cells/well for 96-well plates (Orbach et al. 2018). Briefly, cells were thawed in manufacturer supplied OptiThaw media and plated in OptiPlate. From there, cells were maintained in OptiCulture. CS

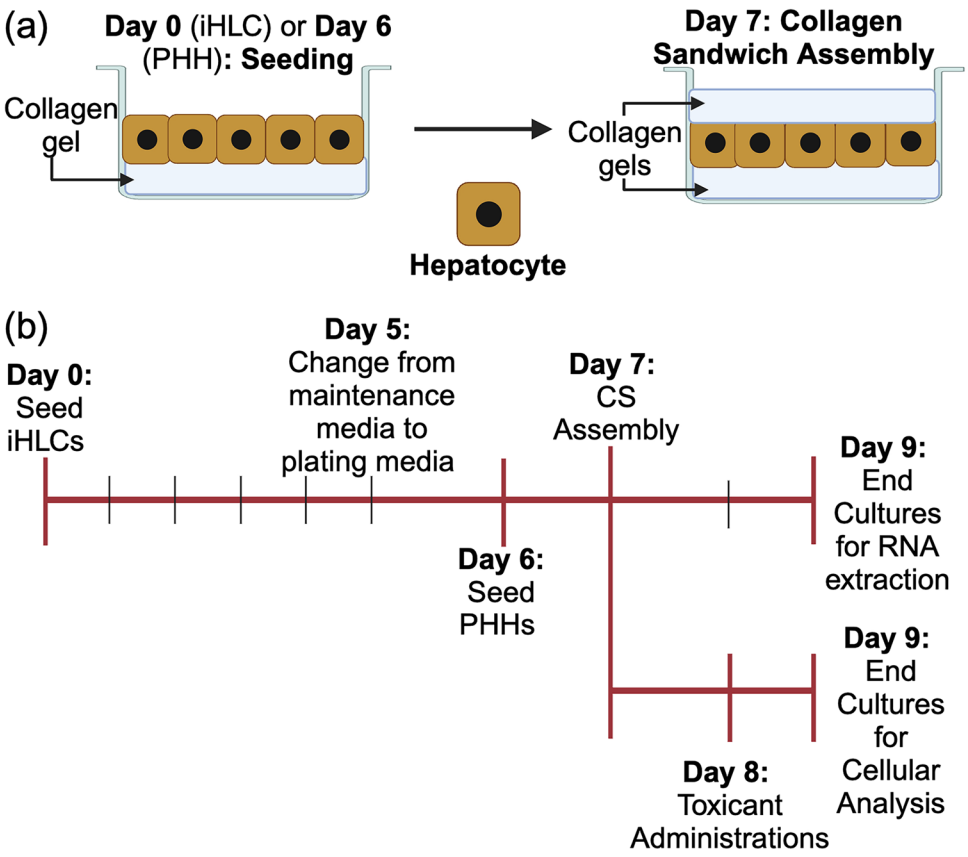

Fig. 1 **a** Assembly of collagen sandwich hepatocyte cultures. **b** Timeline for iHLC and PHH cultures for the RNA-seq experiment

cultures were assembled 24 h post-seeding as previously described (Fig. 1a). Spent culture medium was collected at every 24 h and stored at −80 °C until analyzed. Cells were maintained at 37 °C in a humidified environment at 5% carbon dioxide.

Extraction of RNA from PHHs and iHLCs

RNA extraction was conducted on cells when thawed immediately after cryopreservation as well as from cultured iHLCs and PHHs. The extraction was conducted on cells of the same lot number and donor. The cells were mixed with RNAprotect Cell Reagent (Qiagen, Hilden, Germany) and stored until extraction. iHLC and PHH cultures were detached from collagen-coated TCPS plates upon the addition of TrypLE and collagenase, respectively (Kim et al. 2010; Kim and Rajagopalan 2010; Larkin et al. 2013; Orbach et al. 2018). After centrifugation and aspiration of the supernatant, the remaining pellet was re-suspended in RNAprotect Cell Reagent.

RNA extraction was conducted using the RNeasy Plus Micro Kit (Qiagen) following the manufacturer's protocol. Briefly, cells were suspended in the RNAprotect Cell Reagent, centrifuged, and re-suspended in RLT buffer supplemented with β-mercaptoethanol (14.3 M). The lysate was homogenized using QIAshredder spin columns. The homogenized lysates were transferred to gDNA Eliminator spin columns and the resulting solution was mixed with 70% v/v ethanol. The solution was centrifuged through the RNeasy MinElute spin column. Buffer RW1, Buffer RPE, and 80% v/v ethanol were added sequentially to the spin columns. The final RNA collection step was completed by centrifuging RNase-free water through the spin columns. Samples were stored at −80 °C until further analysis.

RNA-sequencing

The RIN value ranges for samples used in the present study are shown in Table 1. Briefly, the total RNA was converted for sequencing into a strand-specific library using Illumina TruSeq Stranded mRNA HT Sample Prep Kit (Illumina, San Diego, CA) and Illumina's Next Seq/NovaSeq. The cleaved RNA fragments were converted to cDNA using reverse transcriptase and random primers and prepared for library enrichment. After 13 cycles of PCR, 15 individually indexed cDNA libraries were pooled and sequenced on Illumina NextSeq high Output 150 cycle kit to generate approximately 25 million paired-end reads.

Table 1 RIN ranges for samples used in RNA-seq measurements

Sample	RIN range ($n \geq 3$)
iHLCs, day 0	9.6–9.8
iHLCs, day 9	9.7
PHHs, day 6	7.7–8.1
PHHs, day 9	7.5–7.9

Differential gene expression analysis

The RASflow workflow was used for the alignment, gene counting, and differential gene expression analysis of the RNA-seq samples. HISAT2 was used to align RNA-seq reads against the GRCh38 cDNA transcriptome obtained from ENSEMBL (Herrero et al. 2016; Kim et al. 2015; Zhang and Jonassen 2020). Gene counting was performed using the featureCounts program before applying PCA and t-distributed stochastic neighbor embedding (t-SNE) for linear and non-linear dimensionality reduction, and ggplot2 for hierarchical clustering to visualize the resulting gene expression matrix (Jolliffe 2002; Laurens van der Maaten 2008; Liao et al. 2014; Wickham 2011).

Samples for RNA-seq analysis were collected from iHLCs and PHHs on days 0 and 6, respectively, and on day 9 for both cell types. DESeq2 was used to perform differential gene expression analysis (Love et al. 2014). The procedure of Benjamini–Hochberg was applied to adjust for multiple hypothesis testing. Genes with false discovery rate (FDR) adjusted p-values < 0.05 were selected as differentially expressed. ClusterProfiler was used to identify KEGG Pathways and Gene Ontology (GO) Biological Processes enriched in each gene set (Harris et al. 2004; Yu et al. 2012). Enriched terms with p-values < 0.05 were selected as over-represented or under-represented in each comparison.

Administration of toxicants to iHLC and PHH cultures

APAP and EtOH were dissolved in hepatocyte media and administered to cultures 24 h after CS models were assembled (day 8). APAP was administered at 2.5 mM (LC_{50} for humans, lethal concentration 50) and 5 mM ($2 \times LC_{50}$ for humans), respectively (Klaassen 2013; Orbach et al. 2018). EtOH was also added at 80 mM (½ LC_{50} for humans) and 160 mM (LC_{50} for humans) (Klaassen 2013; Orbach et al. 2018).

Immunofluorescence measurements of iHLCs and PHHs

iHLC and PHH cultures were fixed in a 2% (v/v) glutaraldehyde solution in PBS (1×). The cells were then sequentially exposed to a 0.1% (v/v) Triton-X 100 solution in PBS (1×) and a 1% (w/v) BSA/PBS (1×) blocking solution with 1.5% (v/v) goat serum. Intracellular albumin was identified using a primary polyclonal sheep anti-human serum albumin antibody (Abcam, Cambridge, MA) followed by incubating

with a DAPI-conjugated secondary antibody (Thermo Fisher Scientific). Bile canaliculi were identified using a primary monoclonal mouse anti-human CD26 antibody (Thermo Fisher Scientific) followed by a TRITC-conjugated secondary antibody (Abcam). Actin was stained with rhodamine phalloidin (Thermo Fisher Scientific). Imaging was conducted on a Zeiss LSM 880 confocal microscope.

Measurement of urea secretion

Spent culture medium was assayed for the secretion of urea using a colorimetric BUN kit (StanBio Laboratory, Boerne, TX) (Kim et al. 2010; Larkin et al. 2013; Orbach et al. 2017). The urea concentration was determined through absorbance measurements at 520 nm. A standard curve was developed by diluting urea in hepatocyte medium.

Measurement of DNA

DNA measurements were performed using the Quant-iT PicoGreen kit (Thermo Fisher Scientific). iHLCs and PHHs were released from gels by treating cultures with TrypLE or collagenase, respectively. Cell suspensions were collected, pelleted, and re-suspended in a 0.1% (w/v) SDS solution containing EDTA and Tris–HCl. Fluorescence was measured at an excitation/emission wavelength of 480 and 520 nm, respectively (Grant et al. 2019). A standard curve was generated by diluting the provided Lambda DNA. The original sample were diluted 10× in TE buffer prior to being assayed.

Measurement of the activity of cytochrome P450 2E1

Cytochrome P450 2E1 (CYP2E1) activity was measured 24 h after toxicant administration (day 9) (Donato et al. 2004; Orbach et al. 2018). CYP2E1 enzymatic activity was measured through the metabolic conversion of MFC to HFC. Then, 10 µM of MFC was added to the cultures and allowed to incubate at 37 °C for 1 h. The culture medium was collected and combined with β-glucuronidase/arylsulfatase and 0.5 M acetic acid. The mixture was incubated at 37 °C for 2 h. An equivalent volume of a 0.25 N Tris in 60% acetonitrile (v/v) was added to quench the reaction. The concentration of HFC was measured at an excitation/emission wavelength of 410 and 510 nm, respectively, and compared to a standard curve to calculate enzymatic activity.

Measurement of glutathione

Glutathione (GSH) was measured 24 h after toxicant treatment (day 9) using the GSH-Glo Glutathione Assay (Promega, Madison, WI). Cultures were incubated with Luciferin-NT and glutathione S-transferase. Luciferin detection reagent was added to generate a luminescent signal which was compared to controls to determine changes in GSH (Orbach et al. 2018).

Analysis of mitochondrial membrane integrity

Mitochondrial membrane integrity was measured using the JC-1 Mitochondrial Membrane Potential Detection Kit (Biotium, Fremont, CA). The cationic JC-1 dye (5,5′,6,6′-tetrachloro-1,1′,3,3′-tetraethylbenzimidazolylcarbocyanine iodide) was added to the cell cultures 24 h after toxicant administration (day 9) and incubated for 15 min at 37 °C. Fluorescence was measured to determine the numbers of both healthy (red; measured at an excitation/emission wavelength of 550 and 600 nm, respectively) and damaged (green; measured at an excitation/emission wavelength of 485 and 535 nm, respectively) cells. The ratio of red to green determined changes in the mitochondrial membrane integrity, with decreased ratios indicating mitochondrial damage (Orbach et al. 2018).

Statistical analysis

All results are reported as mean ± standard deviation; n represents the sample size. For the experimental analysis, statistical significance was determined using a two-tailed Student's t-test with $\alpha = 0.05$. Unequal variance was assumed. The Bonferroni correction was applied to adjust for testing multiple hypotheses.

Results

Dimensionality reduction and clustering

The timeline for conducting RNA-seq analysis on different cell types is shown in Fig. 1b. We performed hierarchical clustering (Fig. 2a) and dimensionality reduction (Fig. 2b, c) on the RNA-seq data ("Materials and methods" section). We found that the samples first clustered by cell type and subsequently, within each cell type, by timepoint (Fig. 2a). These results indicate that there is a measurable difference in gene expression between both cell types at these time points. PCA and t-SNE analysis visually corroborated this clustering (Fig. 2b, c). The first principal component (PC1) accounts for 89% variance and the second component (PC2) accounts for 8% in the data. PHH samples were substantially separated from iHLC samples along PC1, suggesting that this component correlated with cell type. On the other hand, PHH samples on day 6 were separated from day 9 samples along PC2, as were iHLC samples on days 0 and 9,

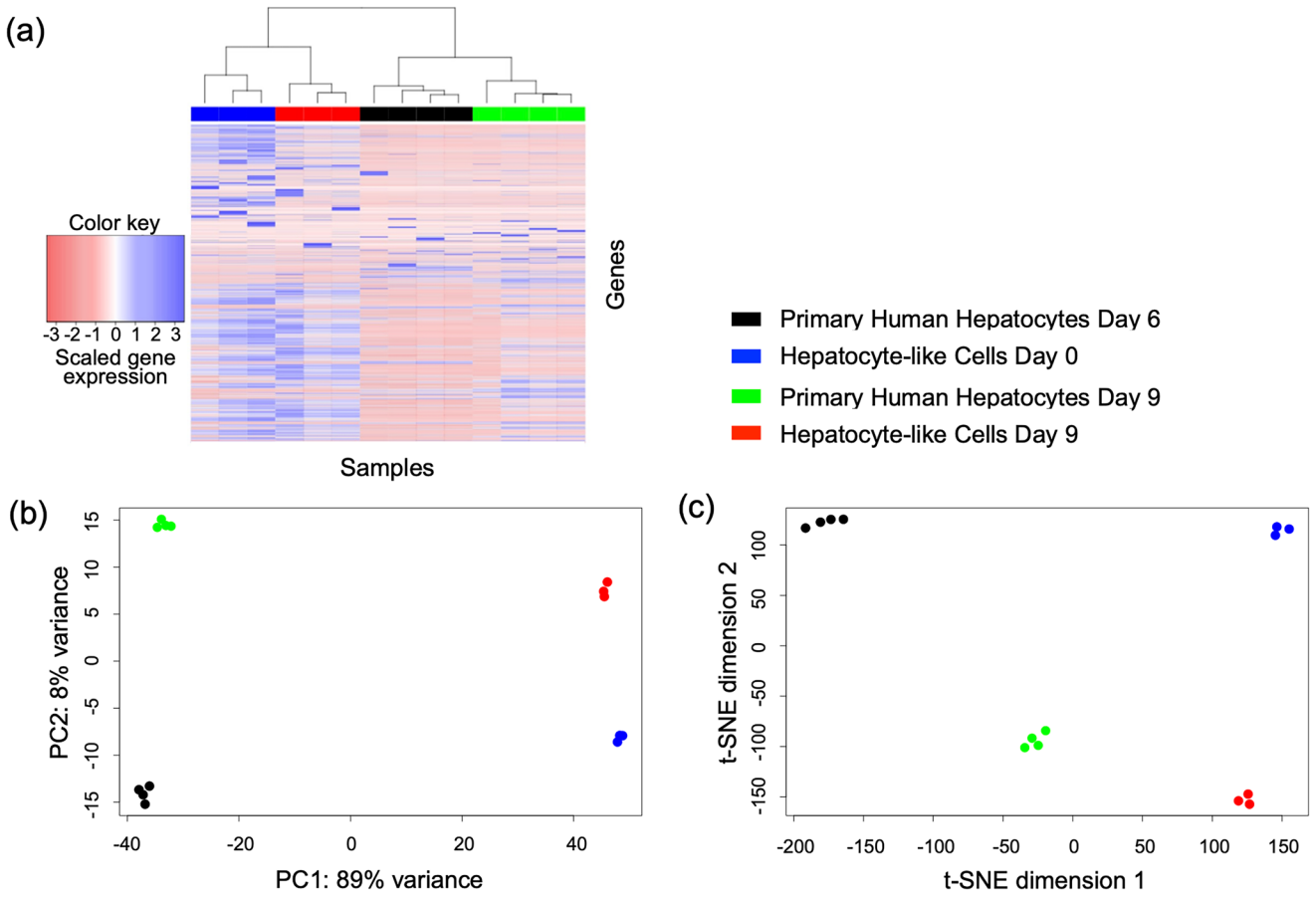

Fig. 2 **a** Hierarchical clustering of PHH and iHLC gene expression data. **b** PCA and **c** t-SNE dimensionality reduction

indicating that this component may correspond to the time-point. Similarly, in the t-SNE plot, biological replicates at each time point were clustered together within these groups and were distinctly separate from samples for other days and cell types.

Differential gene expression analysis and functional enrichment

Encouraged by this result, we computed the genes that were overexpressed in PHHs compared to iHLCs on day 9 ("Materials and methods" section). For this comparison, there were a total of 9504 differentially expressed genes. Functional enrichment analysis in this set of genes ("Materials and methods" section) identified 51 pathways (only 30 are shown) (Fig. 3) overrepresented in PHH samples with a p-value below 0.05 ($p < 0.05$). We further investigated several of these enriched pathways and processes related to hepatic functions.

Bile secretion

Genes involved in bile secretion were upregulated in PHHs compared to iHLCs on day 9. Of the 80 genes in the bile secretion pathway, 44 were found to be upregulated in PHHs ($p < 0.05$). A major function of the liver is the production of bile acids and their transport through bile canaliculi (Arias et al. 2009). Cholesterol causes the synthesis of bile acids, which aid in the absorption and clearance of lipids and lipid-soluble vitamins and molecules (Detzel et al. 2011; Arias et al. 2009). Bile acids are transported and recycled through the liver. Inhibition of this pathway can lead to severe complications, such as gallstones and cholestasis (Detzel et al. 2011).

UDP-glucuronosyltransferase (UGT) genes were upregulated in PHHs. Bile glucuronidation, conducted by UGT enzymes, is an important step in the conjugation of bilirubin to allow for the formation of water-soluble molecules (Barbier et al. 2009). Of note, UGT1A1, the primary enzyme that glucuronates bilirubin to conjugated bilirubin,

was elevated by 15-fold in PHHs (Liu et al. 2021). Aquaporin 9 (AQP9) was upregulated in PHHs by 455-fold. This gene corresponds to a channel on the basolateral membrane of hepatocytes, and facilitates transport of urea, water, glycerol, and bile (Jelen et al. 2012; Marinelli et al. 2011). ATP binding cassette coding genes (ABCB1, ABCG5, ABCC2, ABCB4, ABCG2, ABCC3) were significantly upregulated as well ($p < 0.05$). These ATP-dependent proteins transport molecules across the hepatocyte membrane and are involved in the metabolism of drugs and xenobiotics (Chiang 2013).

We focused on two major enzymes involved in the cholesterol metabolism cascade. CYP7A1, an enzyme found in the endoplasmic reticulum membrane, catalyzes the initial reaction in cholesterol metabolism to bile acids in hepatocytes (Chiang 2013). This is the rate-limiting step in the catabolic pathway (Chiang 2013). PHHs expressed 3.44-fold higher CYP7A1 compared to iHLCs. BAAT, bile acid-CoA amino acid *N*-acyltransferase, catalyzes the second step in bile-acid production from cholesterol (Manley and Ding 2015). This gene was upregulated in PHHs by 3.3-fold. The upregulation of these enzymes suggests that the ability to metabolize cholesterol in iHLCs may be lower than in PHHs. The gene expression analysis was validated by immunofluorescence measurements which show that bile canaliculi were present only in PHHs (Fig. 4a, b). Bile canaliculi are responsible for transporting bile on the apical side of hepatocytes (Arias et al. 2009). ABCB4, ABCG5/8, and bile salt export protein (BSEP or ABCB11) are three key genes that regulate and are involved in the formation of bile and transport through the canaliculi of hepatocytes (Kroll et al. 2021). BSEP is expressed in both cell types. However, there is no statistically significant difference in expression ($p > 0.05$). ABCB4 and ABCG5/8 are expressed 5.4-fold, 8.2-fold, and 5.4-fold higher in PHHs compared to iHLCs. In addition, SLC51A, SLC10A1, and SLCO1B3, members of the solute carrier transporter family, import bile acids in hepatocytes (Kroll et al. 2021). These three genes were upregulated in PHHs by 4.1-, 3.9-, and 41.4-fold higher in PHHs, respectively. The lower expression of these proteins could explain the lack of bile formation and, therefore, the absence of canaliculi in iHLCs (Fig. 4c) (Kroll et al. 2021).

TCA cycle

The TCA cycle was upregulated in PHHs compared to iHLCs on day 9 ($p < 0.05$). Of the 29 genes in this KEGG pathway, 19 genes were upregulated in PHHs. These genes corresponded to five out of the eight steps involved in the citric acid cycle (Table 2) (Akram 2014).

The most upregulated gene in the TCA cycle pathway was PCK1 (phosphoenolpyruvate carboxykinase 1), the primary regulator of gluconeogenesis (Rui 2014). Gluconeogenesis can occur as a result of a low insulin-to-glucagon ratio and by downstream signaling through cAMP pathways to produce glucose (Rui 2014). PCK1 was elevated by 87-fold in PHHs compared to iHLCs. This enzyme catalyzes the formation of phosphoenolpyruvate from oxaloacetate, derived from pyruvate (Rui 2014; Stark et al. 2009). This enzyme also promotes the TCA cycle by removing metabolic waste and contributing to pyruvate cycling, or the production of pyruvate to make ATP for the cell by initiating the citric acid cycle when glucose is low (Fig. 4d) (Montal et al. 2019; Wang and Dong 2019). PCK1 expression is regulated transcriptionally, post-transcriptionally, and post-translationally (Xiang et al. 2023; Yu et al. 2021). However, the most common mechanism is transcriptional regulation (Xiang et al. 2023; Yu et al. 2021). Acetylation, ubiquitination, SUMOylation, and phosphorylation may also regulate the activity of PCK1 (Xiang et al. 2023; Yu et al. 2021). The translational regulation of rate-limiting enzymes, such as PCK1, may contribute to the differences exhibited in the gene expression and urea secretion in iHLCs compared to PHHs.

In addition, OGDHL, or oxoglutarate dehydrogenase L, was upregulated in PHHs by 63.5-fold. OGDHL also downregulates protein kinase B (AKT) signaling cascades (Madhunapantula et al. 2011). AKT signaling can be coupled with phosphoinositide 3-kinase (PI3K) and the mammalian target of rapamycin (mTOR), which is involved in cell proliferation, migration, and protein and glucose metabolism (Madhunapantula et al. 2011). The PI3K/AKT/mTOR pathway is also involved in regulating glucose levels (Madhunapantula et al. 2011).

The transamination of oxaloacetate produces aspartate which reacts with citrulline to feed into the urea cycle (Shambaugh 1977). We evaluated urea secretion as a metric for PHH and iHLC function (Kim and Rajagopalan 2010; Larkin et al. 2013). The experimental results show normalized urea secretion in PHHs is 2- to 2.5-fold higher than in iHLCs on days 8 and 9 in culture ($p < 0.05$, Fig. 4e).

Hepatic biotransformation

The CYP450 family of enzymes are primarily responsible for biotransformation, an important liver function that involves the metabolism of harmful toxicants and xenobiotics that enter the body (Wills and Rajagopalan 2020; Arias et al. 2009). Although several CYP450 enzymes are present in the liver, CYP3A4, CYP2C9, CYP2C19, CYP2D6, CYP1A2, and CYP2E1 are responsible for the majority of drug and toxicant metabolism (Leung and Nieto 2013; Wills and Rajagopalan 2020). Genetic polymorphisms in these enzymes are responsible for the variability to drug responses between individuals (Zanger and Schwab 2013). The UGT enzymes are also responsible for drug as well as

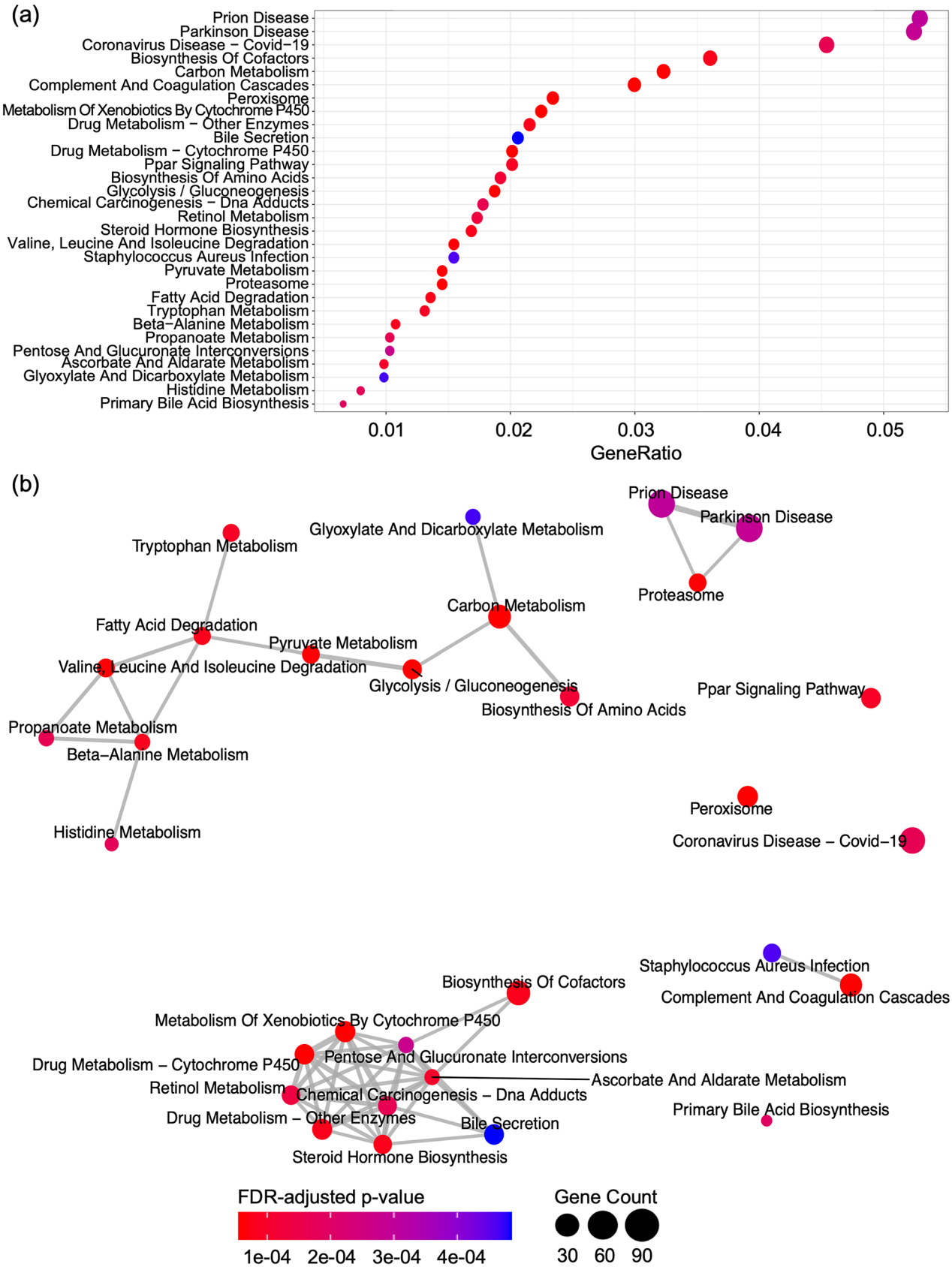
(a)
Prion Disease
Parkinson Disease
Coronavirus Disease – Covid–19
Biosynthesis Of Cofactors
Carbon Metabolism
Complement And Coagulation Cascades
Peroxisome
Metabolism Of Xenobiotics By Cytochrome P450
Drug Metabolism – Other Enzymes
Bile Secretion
Drug Metabolism – Cytochrome P450
Ppar Signaling Pathway
Biosynthesis Of Amino Acids
Glycolysis / Gluconeogenesis
Chemical Carcinogenesis – Dna Adducts
Retinol Metabolism
Steroid Hormone Biosynthesis
Valine, Leucine And Isoleucine Degradation
Staphylococcus Aureus Infection
Pyruvate Metabolism
Proteasome
Fatty Acid Degradation
Tryptophan Metabolism
Beta–Alanine Metabolism
Propanoate Metabolism
Pentose And Glucuronate Interconversions
Ascorbate And Aldarate Metabolism
Glyoxylate And Dicarboxylate Metabolism
Histidine Metabolism
Primary Bile Acid Biosynthesis
0.01
0.02
0.03
0.04
0.05
GeneRatio
(b)
Prion Disease
Parkinson Disease
Proteasome
Glyoxylate And Dicarboxylate Metabolism
Tryptophan Metabolism
Carbon Metabolism
Fatty Acid Degradation
Pyruvate Metabolism
Valine, Leucine And Isoleucine Degradation
Glycolysis / Gluconeogenesis
Biosynthesis Of Amino Acids
Ppar Signaling Pathway
Propanoate Metabolism
Beta–Alanine Metabolism
Peroxisome
Histidine Metabolism
Coronavirus Disease – Covid–19
Staphylococcus Aureus Infection
Biosynthesis Of Cofactors
Complement And Coagulation Cascades
Metabolism Of Xenobiotics By Cytochrome P450
Drug Metabolism – Cytochrome P450
Pentose And Glucuronate Interconversions
Ascorbate And Aldarate Metabolism
Retinol Metabolism
Chemical Carcinogenesis – Dna Adducts
Primary Bile Acid Biosynthesis
Drug Metabolism – Other Enzymes
Bile Secretion
Steroid Hormone Biosynthesis
FDR-adjusted p-value
1e-04
2e-04
3e-04
4e-04
Gene Count
30
60
90

◂**Fig. 3** **a**, **b** KEGG pathways upregulated in PHHs compared to iHLCs on day 9. **a** Each row represents a KEGG pathway. The *x*-axis corresponds to the fraction of genes in the pathway that are also differentially expressed. The legend for the color and size of the circles appears in the right of the panel. **b** Network of overlaps between enriched pathways. Each node is a pathway, and each edge connects pairs of pathways that overlap in differentially expressed genes. Node color indicates the FDR-corrected *p*-value of enrichment for the corresponding pathways while node size reflects the number of genes in the pathway

bilirubin metabolism and hormone degradation (Maruo et al. 2005). Polymorphisms in these enzymes can also contribute to adverse reactions to several non-polar, lipophilic drugs (Maruo et al. 2005; Rowland et al. 2013).

Three KEGG pathways related to biotransformation were upregulated in PHHs compared to iHLCs on day 9 (Table 3). Since the pathways had upregulated genes in common with each other, we discuss the differential gene expression of enzymes responsible for drug metabolism from all three pathways, with a focus on CYP450 and UGT enzyme families.

CYP450 enzymes

CYP450 enzymes are heme-containing proteins that catalyze the metabolism of various xenobiotics, drugs, carcinogens, steroids, eicosanoids, and vitamins (Arias et al. 2009; Zanger and Schwab 2013). The metabolism of these compounds by CYP450 enzymes can result in reactive metabolites which can cause liver injury (Leung and Nieto 2013; Orbach et al. 2018; Arias et al. 2009; Zanger and Schwab 2013). The fold changes in gene expression between PHHs and iHLCs of CYP enzymes involved in the three KEGG pathways are presented in Table 4. CYP1A2 is one isoform of the CYP1 family, which also includes CYP1A1 and CYP1B1 (Klein et al. 2010). CYP1A2 metabolizes drugs, such as clozapine, used in the treatment of neurological conditions (Klein et al. 2010). The gene expression level of CYP1A2 was 8254-fold higher in PHHs compared to iHLCs. While the expression of 11 CYP enzymes was upregulated, we focused our investigation on two toxicants metabolized by CYP2E1. We specifically investigated CYP2E1 because it is the primary enzyme involved in the metabolism of APAP and EtOH, two common toxicants that can lead to significant liver damage, and was shown to be upregulated 21,810-fold in PHHs compared to iHLCs at day 9 (David and Hamilton 2010; Kuna et al. 2018; Orbach et al. 2017, 2018). APAP is one of the leading causes of acute liver failure in the USA and ethanol can lead to a variety of liver diseases, including alcoholic fatty liver disease, fibrosis, and death (David and Hamilton 2010; Orbach et al. 2017).

The activity of CYP enzymes, such as CYP2E1, can result in the production of reactive oxygen species (ROS) (Lu and Cederbaum 2008). Although ROS are produced by several reactions in the body, the build-up of these molecules can cause severe damage to cells by denaturing proteins, damaging RNA, DNA, and deactivating enzymes (Guo et al. 2013; Leung and Nieto 2013). Therefore, antioxidants such as GSH prevent damage caused by ROS through enzymatic and non-enzymatic mechanisms (Leung and Nieto 2013). Generally, there is a balance between free radicals and neutralizing molecules. When disrupted, an increase of ROS causes a depletion of GSH, which leads to oxidant stress and cellular damage (Orbach et al. 2018).

Mitochondria, peroxisomes, and smooth endoplasmic reticulum (ER) are the three organelles in hepatocytes that produce the most ROS (Leung and Nieto 2013). CYP2E1 is primarily located in the ER and mitochondria of hepatocytes (Neve and Ingelman-Sundberg 2000). The production of ROS affects the mitochondrial respiratory chain, which aids in the production of cellular ATP (Guo et al. 2013). These free radicals directly damage the complexes involved in the electron-transport chain in addition to proteins, lipids, and DNA (Guo et al. 2013). This cascading effect can lead to the damage of mitochondria by decreased transcription and translation of mitochondrial proteins, increased permeability of the organelle membrane, and the release of cytochrome C and apoptosis (Guo et al. 2013) (Fig. 5a).

To further evaluate CYP2E1 activity in PHHs and iHLCs, we measured the formation of HFC when APAP and EtOH were administered to cultures (Donato et al. 2004; Orbach et al. 2018). Two concentrations of APAP, 2.5 mM (LC_{50} for humans) and 5 mM ($2 \times LC_{50}$), and EtOH, 80 mM (1/2 LC_{50}) and 160 mM (LC_{50}), were administered. For each of the concentrations, there was a statistically significant difference ($p < 0.05$) in CYP2E1 activity in PHHs compared to iHLCs. The baseline CYP2E1 activity in PHHs was $1.16 \times 10^{-5} \pm 0.321 \times 10^{-5}$ pmol/min/cell compared to $0.317 \times 10^{-5} \pm 0.00827 \times 10^{-5}$ in iHLCs, representing an approximate 3.7-fold change (Fig. 5b, c). CYP2E1 activity in PHHs was 4.30-fold and 3.79-fold higher than in iHLCs at 2.5 and 5 mM APAP, respectively. Similarly, after ethanol administration, CYP2E1 activity for PHHs was 4.12-fold and 6.20-fold higher than in iHLCs for EtOH concentrations of 80 and 160 mM, respectively.

Regulation of CYP2E1 occurs through transcriptional, post-transcriptional, translational, and post-translation mechanisms (Fig. 5f). However, activity of this enzyme most commonly occurs due to post-transcriptional events (Novak and Woodcroft 2000). For example, a study by Kocarek et al. indicated that the CYP2E1 mRNA has high turnover and is not immediately degraded upon translation (Kocarek et al. 2000; Novak and Woodcroft 2000). The turnover is translation dependent, indicating that the same mRNA strand may yield high quantities of the protein (Kocarek et al. 2000; Novak and Woodcroft 2000). The structure of the CYP2E1 mRNA can also affect protein synthesis (Kocarek et al. 2000;

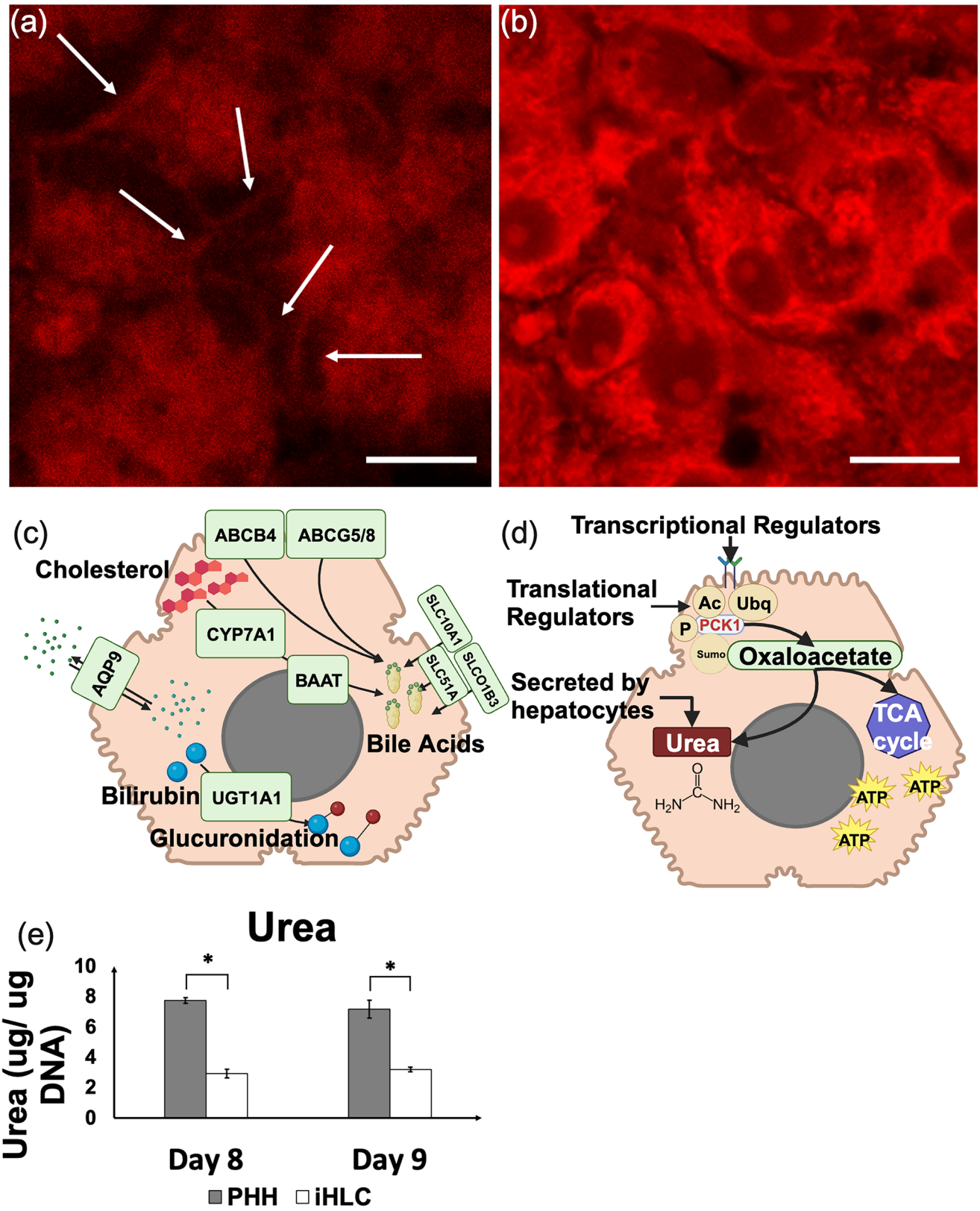

Fig. 4 Immunostaining of bile canaliculi on day 9 for **a** PHHs and **b** iHLCs. White arrows point to bile canaliculi. Scale bars = 50 μ m. **c** Schematic of key proteins regulating bile secretion and bile canaliculi formation in hepatocytes. **d** Schematic of PCK1 regulating oxaloacetate which feeds into the TCA and urea cycles. **e** Urea secretion of PHHs and iHLCs at day 8 and day 9. $*p < 0.05$ relative to the iHLCs values at each respective time point, $n \geq 3$

Table 2 Upregulated genes corresponding to enzymes in TCA cycle in PHHs compared to iHLCs

Enzyme corresponding to step in TCA cycle	Fold-change in PHHs vs. iHLCs
ACO1/ACO2 (aconitase)	1.990/1.891
IDH2/IDH3G (isocitrate dehydrogenase)	1.542/4.968
SDHB (succinyl-CoA dehydrogenase)	1.536
FH (fumarase)	2.073
MDH1/MDH2 (malate dehydrogenase)	2.108/2.160

Novak and Woodcroft 2000). Proteinases that modify mRNA and deplete the 5′ UTR end resulted in increased CYP2E1 expression (Kocarek et al. 2000; Novak and Woodcroft 2000). The poly(A) tail of the CYP2E1 mRNA and sequences in the 3′ UTR sequence protect from RNase activity and degradation (Kocarek et al. 2000; Novak and Woodcroft 2000). These mechanisms may explain the drastic differences observed between the activity and fold-change of CYP2E1 in iHLCs and PHHs (Kocarek et al. 2000; Novak and Woodcroft 2000; Orbach et al. 2018).

Mitochondrial membrane integrity was also studied to understand the effects of CYP2E1 metabolism (Fig. 5d, e) for cultures treated with APAP and EtOH (Orbach et al. 2018; Sivandzade et al. 2019). A decrease in the JC-1 ratio is an indication of increased mitochondrial membrane damage (Orbach et al. 2018). For both toxicants, the ratio was decreased in iHLCs compared to PHHs; however, the difference was not statistically significant ($p < 0.05$). We also measured GSH fold changes in APAP and EtOH-treated samples; however, changes in GSH were statistically insignificant. The RNA-seq analysis concluded that the GSTT1 gene, a glutathione transferase enzyme, had a 19,860-fold change in PHHs compared to iHLCs. More investigation on glutathione depletion due to biotransformation in each cell type is needed.

UDP-glucuronosyltransferase enzymes

UGT enzymes are involved in the metabolism of bilirubin, hormones, and vitamins (Allain et al. 2020; Maruo et al. 2005). Here, we report their upregulation in PHHs compared to iHLCs with respect to the drug metabolism pathways. UGT enzymes are involved in conjugation reactions in biotransformation of toxicants and xenobiotics (Allain et al. 2020). Glucuronidation reactions occur because of UGT enzymes, where glucuronic acid is covalently linked to a substrate, which neutralizes metabolic activity and aids in elimination (Allain et al. 2020). UGT1A10 was the most upregulated UGT enzyme in the pathways with a 2618.5-fold change in PHHs compared to iHLCs. UGT2B17 was differentially expressed with a 679-fold change. More investigation of glucuronidation reactions in iHLC drug metabolism is needed. In addition, the versatility of these enzymes warrants further investigation on their involvement in multiple pathways (Allain et al. 2020).

Table 3 KEGG pathways involved in drug metabolism upregulated in PHHs compared to iHLCs at day 9

KEGG pathway	Upregulated genes/ total genes in pathway	*p*-value
Metabolism of xenobiotics by CYP450	48/66	4.61×10^{-9}
Drug metabolism—CYP450	43/61	1.81×10^{-7}
Drug metabolism—other enzymes	46/76	2.18×10^{-5}

Table 4 CYP450 enzymes upregulated in the KEGG drug metabolism pathways and the fold changes in PHHs compared to iHLCs

CYP450 enzyme	Fold change in PHHs compared to iHLCs
CYP2C9	36.362
CYP2E1	21,810.944
CYP1A2	8254.906
CYP2A6	39,409.052
CYP2B6	18,165.926
CYP1A1	7.648
CYP2A7	1811.516
CYP2D6	494.059
CYP2S1	10.086
CYP2A13	36.722
CYP1B1	3.831

Actin organization

Hepatocytes require organized actin filaments to self-assemble (Tzanakakis et al. 2001). The actin cytoskeleton is usually confined to the peripheral regions in PHHs (Fig. 6a) (Kim et al. 2010). However, the actin cytoskeleton in iHLCs was observed throughout the cross-section of the cell (Fig. 6b). The dedifferentiation of hepatocytes can result in the organization of actin stress fibers that span the entire cell (Kim et al. 2010; Roy-Chowdhury et al. 2017). PHHs have a 1.32-fold difference in the ACTB, the actin gene, compared to iHLCs, which could explain the difference in the actin cytoskeleton.

Intracellular albumin expression

Albumin is used as a marker for hepatic maturation, specifically in studies on the differentiation of iHLCs (Si-Tayeb et al. 2010; Wills and Rajagopalan 2020). Based on immunofluorescence images, the expression of intracellular albumin appears to be

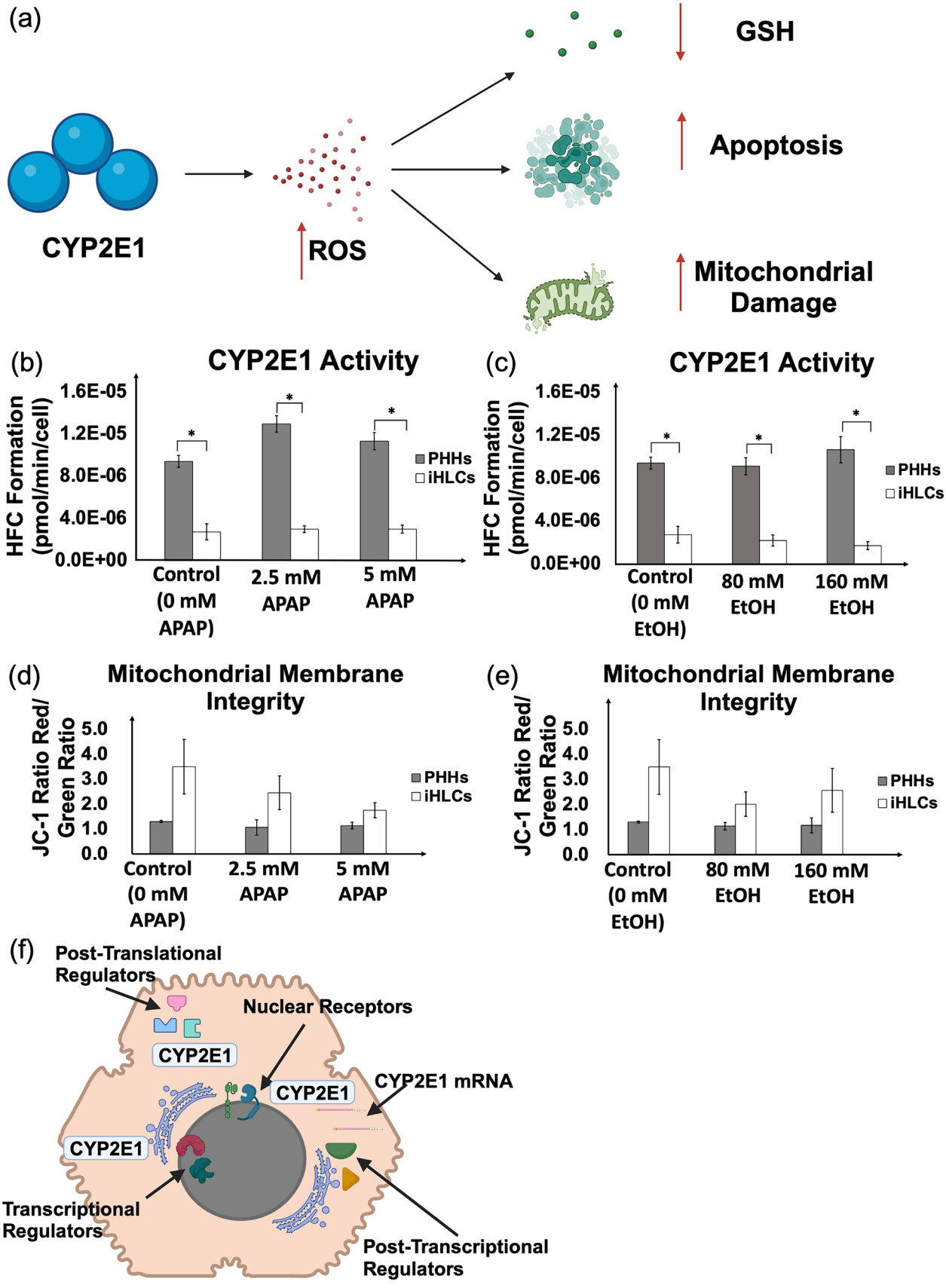
(a)
GSH
Apoptosis
Mitochondrial Damage
CYP2E1
ROS
(b)
CYP2E1 Activity
HFC Formation (pmol/min/cell)
1.6E-05
1.2E-05
8.0E-06
4.0E-06
0.0E+00
PHHs
iHLCs
Control (0 mM APAP)
2.5 mM APAP
5 mM APAP
(c)
CYP2E1 Activity
HFC Formation (pmol/min/cell)
PHHs
iHLCs
Control (0 mM EtOH)
80 mM EtOH
160 mM EtOH
(d)
Mitochondrial Membrane Integrity
JC-1 Ratio Red/ Green Ratio
5.0
4.0
3.0
2.0
1.0
0.0
PHHs
iHLCs
Control (0 mM APAP)
2.5 mM APAP
5 mM APAP
(e)
Mitochondrial Membrane Integrity
JC-1 Ratio Red/ Green Ratio
PHHs
iHLCs
Control (0 mM EtOH)
80 mM EtOH
160 mM EtOH
(f)
Post-Translational Regulators
Nuclear Receptors
CYP2E1
CYP2E1
CYP2E1
CYP2E1 mRNA
Transcriptional Regulators
Post-Transcriptional Regulators

◂**Fig. 5** **a** When ethanol and acetaminophen are administered to hepatocytes, CYP2E1-mediated biotransformation can result in an increase in ROS, which then causes a depletion of GSH and increases in apoptosis and mitochondrial membrane damage. After APAP and EtOH administration to iHLCs and PHHs on day 8. Data is shown for day 9. **b** CYP2E1 activity measured by HFC formation after APAP administration; **c** CYP2E1 activity measured by HFC formation after EtOH administration; **d** red/green JC-1 ratio after APAP administration; **e** red/green JC-1 ratio after EtOH administration. $*p < 0.05$ relative to the iHLC values for each respective culture model, $n \geq 3$. **f** Schematic of different regulators of CYP2E1 enzymes in hepatocytes

similar between iHLCs and PHHs (Fig. 6c, d). The albumin gene, ALB, is not differentially expressed between these cell types, which could explain the experimental results.

Developmental pathways and transcriptional regulators in iHLCs

The phenotypic and transcriptomic analyses in the present study indicate that iHLCs have lower liver-related functions compared to PHHs. We sought to determine if any developmental pathways were upregulated in iHLCs compared to PHHs on day 9. Functional enrichment analysis did not reveal any such pathways in the KEGG database. However, the Wnt signaling pathway in the GO database was significantly upregulated at this time point ($p < 0.05$) in iHLCs (Fig. 7). The activation of this pathway is key in differentiating iPSCs to the definitive endoderm, leading cells toward the hepatic lineage (Krumm et al. 2022; Mallanna and Duncan 2013; Sauer et al. 2014; Si-Tayeb et al. 2010; Takebe et al. 2013). In addition, the Wnt pathway is activated during embryogenesis and regulates hepatobiliary development as well as adult liver regeneration (Perugorria et al. 2019). This pathway is active when hepatocytes are not maintaining hepatic homeostasis or when they may require additional maturation (Perugorria et al. 2019).

In addition, transcription factors including FOXA3, ATF5, CEBPA, FOXA1, GATA4, and GATA6 were significantly downregulated ($p < 0.05$) between iHLCs and PHHs. These transcription factors are reported to be highly expressed

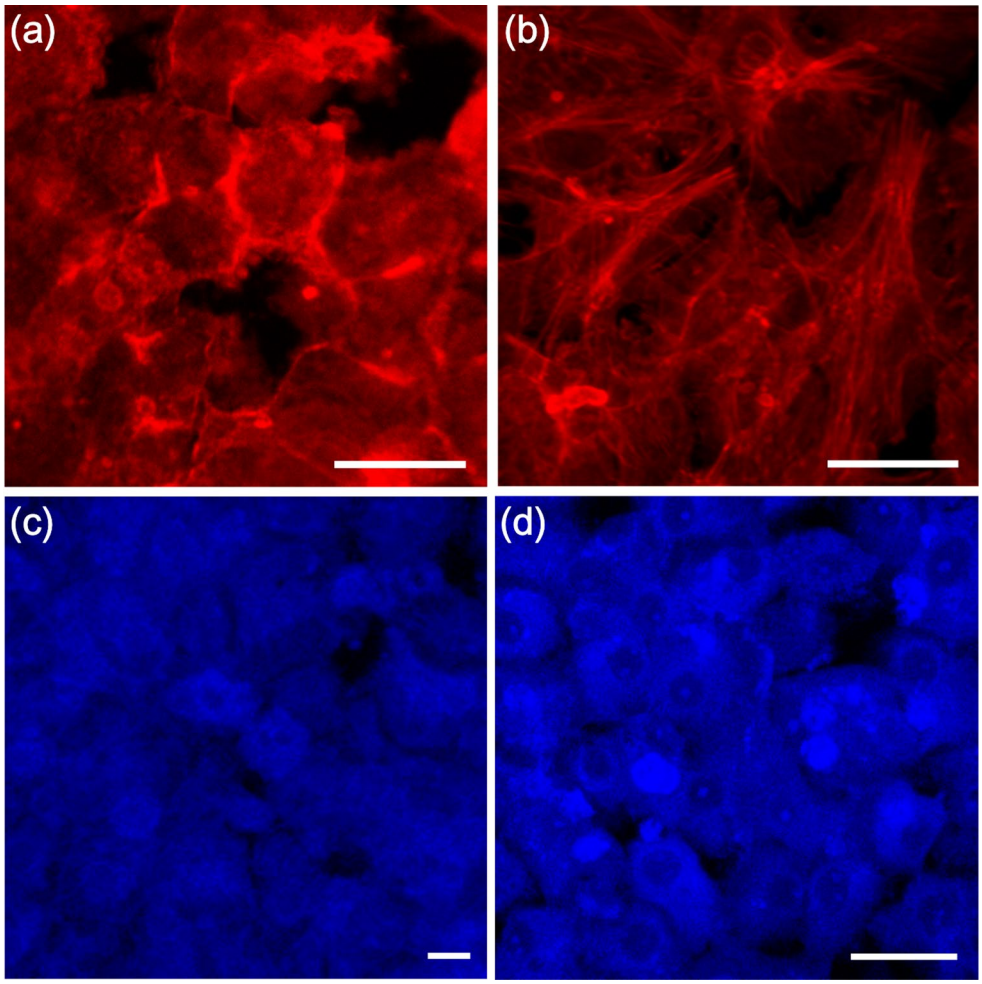

Fig. 6 Immunostaining of the actin cytoskeleton in **a** PHHs and **b** iHLCs on day 9. Immunostaining for albumin in **c** PHHs and **d** iHLCs on day 9. Scale bars = 50 μ m

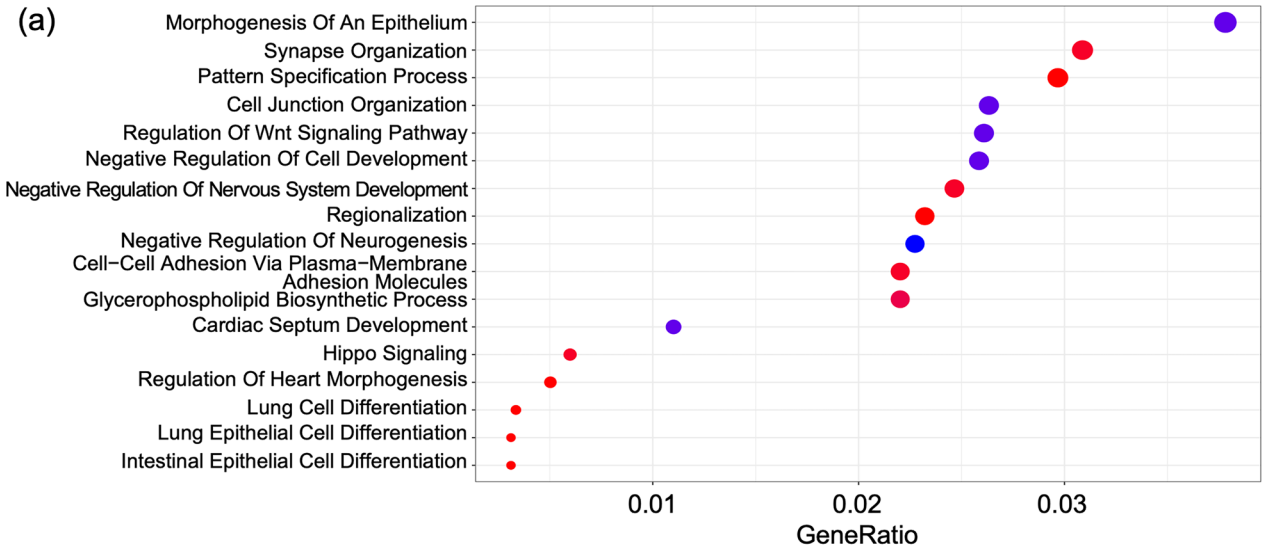
(a)
Morphogenesis Of An Epithelium
Synapse Organization
Pattern Specification Process
Cell Junction Organization
Regulation Of Wnt Signaling Pathway
Negative Regulation Of Cell Development
Negative Regulation Of Nervous System Development
Regionalization
Negative Regulation Of Neurogenesis
Cell−Cell Adhesion Via Plasma−Membrane Adhesion Molecules
Glycerophospholipid Biosynthetic Process
Cardiac Septum Development
Hippo Signaling
Regulation Of Heart Morphogenesis
Lung Cell Differentiation
Lung Epithelial Cell Differentiation
Intestinal Epithelial Cell Differentiation
0.01
0.02
0.03
GeneRatio

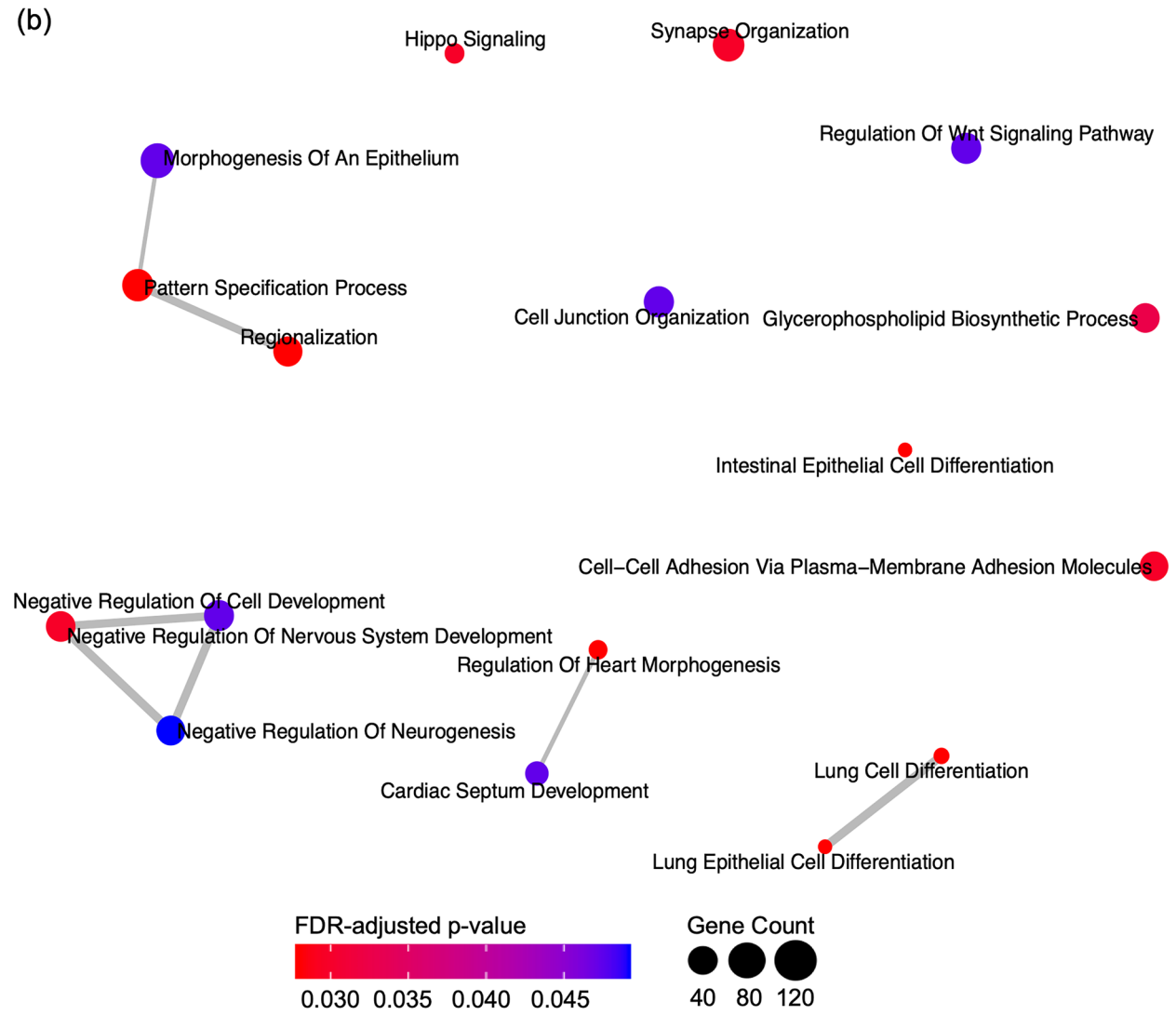
(b)
Hippo Signaling
Synapse Organization
Regulation Of Wnt Signaling Pathway
Morphogenesis Of An Epithelium
Pattern Specification Process
Regionalization
Cell Junction Organization
Glycerophospholipid Biosynthetic Process
Intestinal Epithelial Cell Differentiation
Cell−Cell Adhesion Via Plasma−Membrane Adhesion Molecules
Negative Regulation Of Cell Development
Negative Regulation Of Nervous System Development
Regulation Of Heart Morphogenesis
Negative Regulation Of Neurogenesis
Cardiac Septum Development
Lung Cell Differentiation
Lung Epithelial Cell Differentiation
FDR-adjusted p-value
0.030 0.035 0.040 0.045
Gene Count
40 80 120

◂**Fig. 7** **a**, **b** GO pathways upregulated in PHHs compared to iHLCs on day 9. **a** Each row represents a GO pathway. The *x*-axis corresponds to the fraction of genes in the pathway that are also differentially expressed. The legend for the color and size of the circles appears in the right of the panel. **b** Network of overlaps between enriched pathways. Each node is a pathway, and each edge connects pairs of pathways that overlap in differentially expressed genes. Node color indicates the FDR-corrected *p*-value of enrichment for the corresponding pathways while node size reflects the number of genes in the pathway

during liver embryogenesis and regeneration (Du et al. 2014; Nakamori et al. 2017; Xie et al. 2021). These transcription factors further differentiate hepatoblasts to mature hepatocytes (Du et al. 2014; Nakamori et al. 2017; Xie et al. 2021). In maturation protocols, such transcription factors have been added to iHLCs by lentivirus plasmid infection to further induce hepatic lineage (Du et al. 2014; Nakamori et al. 2017; Xie et al. 2021). However, studies vary between which factors effectively lead to maturation since some combinations have resulted in varying phenotypes, rather than a homogenous iHLC population (Du et al. 2014; Nakamori et al. 2017; Orge et al. 2020; Xie et al. 2021).

Discussion

While iHLCs have potential for future in vitro liver studies, it is known that they do not exhibit the same levels of hepatic functionality as PHHs (Viiri et al. 2019; Wills and Rajagopalan 2020). In particular, the differences in their transcriptional programs have not been studied in detail. In this study, we present an RNA-seq analysis comparing PHHs and iHLCs on day 9. Hierarchical clustering, PCA, and t-SNE visualizations of the gene expression profiles showed clear separation between these cell types, indicating that their transcriptional programs may be considerably dissimilar. We used unbiased computational analysis to find specific pathways that are differentially expressed between the two cell types. We reported pathways that impact key functions of hepatocytes, including bile secretion, the citric acid cycle, and biotransformation pathways. The transcriptomic results were validated by cellular analysis, which provides additional unique insights to understanding the differences between iHLCs and PHHs. This study has reported that iHLCs require additional maturation before they can be used instead of PHHs. We have identified several genes that are downregulated in iHLCs in comparison to PHHs that may have contributed to the lower liver functions exhibited. Additional maturation protocols may need to be utilized with iHLCs in order for them to exhibit the same levels of hepatic functions as PHHs. A potential route to mature iHLCs could be the administration of growth factor cocktails to target the downregulated genes. For example, FGF-19 could be added to cultures to target the farnesoid X receptor (FXR) receptor that leads to bile canaliculi formation (Jansen 2017). Oncostatin M and dexamethasone may also be added to increase CYP450 enzyme expression (Lindley et al. 2002; Xie et al. 2021; Zhang et al. 2012).

Since bile canaliculi are only present in PHHs but not iHLCs, the absence could be explained by the lower expression of key enzymes in the bile formation, glucuronidation, and cholesterol metabolism cascades. RNA-seq analyses from polarized iHLCs on Transwell filters report the upregulation of the FXR/retinoid X receptor pathways, involved in bile acid metabolism, compared to non-polarized iHLCs (Dao Thi et al. 2020). Bile acids are typically secreted from the apical membrane of hepatocytes (Dao Thi et al. 2020). Other studies have also shown that polarized iHLCs can lead to more bile functions (Overeem et al. 2019; Ramli et al. 2020).

The lower expression of enzymes in the TCA cycle could explain the differences observed in urea secretion between the two cell types. With less enzymatic activity in the TCA cycle, a lack of buildup of oxaloacetate could yield lower transamination to aspartate, which feeds into the urea cycle. The lower expression of OGDHL downregulates the PI3K/AKT/mTOR pathway, which is involved in maintaining glucose metabolism (Madhunapantula et al. 2011). Acetyl-CoA is derived from pyruvate, the final product of the glycolysis pathway, and is a regulator of both the TCA and urea cycle (Anand and Anand 1999; Shambaugh 1977). Acetyl-CoA is also a regulator for carbamoyl phosphate synthetase 1, the enzyme that catalyzes the first step in urea production (Anand and Anand 1999). Without acetyl-CoA production, the urea cycle would be halted as a result of lack of enzymatic regulation (de Cima et al. 2015). Therefore, the lower gene expression of these enzymes could explain why the urea secretion in iHLCs was lower compared to PHHs.

It has been well established that iHLCs do not have the same CYP activity as PHHs (Gao and Liu 2017; Sjogren et al. 2014). There was a 3.8–39,409-fold change in CYPs that were upregulated in the three biotransformation pathways investigated (Table 4). Interestingly, in our analysis, CYP3A4 was not upregulated in PHHs compared to iHLCs. CYP3A4 is the most abundant enzyme in the liver, metabolizing antidepressants, antibiotics, steroids, and anti-HIV agents (Viiri et al. 2019; Zhou et al. 2007). In the future, we will conduct cellular measurements to determine if these trends hold.

We focused our analysis on CYP2E1, which was upregulated in PHHs by a factor of 2.18×10^4 compared to iHLCs. CYP2E1 has been implicated in APAP and EtOH metabolism, which have been widely studied in in vitro liver models (Liu et al. 2005; Orbach et al. 2017, 2018). Since CYP2E1 activity was decreased in iHLCs, the lack of enzyme activity may explain why there were no significant differences in the JC-1 ratio. The cascading effect from this enzyme leads to

mitochondrial damage and depletion of glutathione caused by the production of ROS (Liu et al. 2005).

Gene expression of liver enzymes, specifically CYP450 enzymes, is idiosyncratic (Choudhury et al. 2017; Preissner et al. 2013). More than 2000 single nucleotide polymorphisms (SNPs) have been identified within CYP450 enzymes which could contribute to vast differences in drug response and clearance among individuals (Choudhury et al. 2017; Preissner et al. 2013). For example, a SNP mutation in the CYP3A4 gene could result in reduced enzyme activity (Guttman et al. 2019). It could be possible that variations in differentiation protocols contribute to differences in fold changes of certain genes between studies. For example, Viiri et al. reported significant differences in CYP1A1 expression in iHLCs derived from protocols that used two different chemical cocktails (Viiri et al. 2019). Genetic reprogramming, another differentiation protocol, of iHLCs with FOXA2 and HNF4α resulted in unstable phenotypes (Orge et al. 2020). In addition, the donor's background can significantly impact gene expression and phenotypic data during experimentation, which is also a challenge when using PHHs for in vitro studies (Godoy et al. 2013). iHLCs can be derived easily from the skin, allowing for multiple sustainable sources for potential patient-specific toxicity studies (Shi et al. 2017). However, the results from this study and others exhibit the significant differences in several genes, pathways, and functions between iHLCs and PHHs, indicating that these cells require significant maturation before their widespread use (Gao and Liu 2017; Sjogren et al. 2014; Viiri et al. 2019).

In the present study, only transcriptomic data conducted with bulk RNA-seq was examined. Although, other 'omic data may also be investigated. Viiri et al. used GRO-Seq to investigate differences in nascent RNAs including long non-coding RNA, primary miRNAs, and transcription factor binding sites of all lncRNAs (Viiri et al. 2019). The mRNA results from Virii et al. and the present study show some overlap. For example, CYP2E1, CYP1A1, CYP1A2, CYP2C9, and CYP2A6 were significantly upregulated in PHHs in both studies (Viiri et al. 2019). In addition, we have identified 13 UGT enzymes that were upregulated in PHHs compared to iHLCs, which were also reported by Viiri et al. (Viiri et al. 2019). Since iHLCs can be derived by various methods and donors, additional 'omics analyses could provide a deeper understanding of the differences between the two cell types.

In addition to bulk RNA-seq methods, individual cell differences in the transcriptomic programs of iHLCs and PHHs have also been investigated using single cell RNA-sequencing (scRNA-seq), which can be used to understand heterogeneity of a population (Brazovskaja et al. 2019; Chen et al. 2020; Nell et al. 2022; Shinozawa et al. 2021). These studies differ in the ways they induce the differentiation of iPSCs or progenitor cells into iHLCs, whether they incorporate iHLCs into organoids or not, or in their source for PHHs. Nevertheless, they point to similar trends between iHLCs and PHHs, especially the fact that protocols to create iPSCs often yield cells with characteristics of fetal hepatocytes (Camp et al. 2017; Nell et al. 2022; Shinozawa et al. 2021; Wesley et al. 2022).

One study compared scRNA-seq measurements of human liver organoids derived from storable foregut progenitors (themselves induced from iPSCs) and PHHs (Shinozawa et al. 2021). The organoids included hepatocyte-like cells that were virtually identical to PHHs and non-parenchymal cells (Shinozawa et al. 2021). However, half the cells were in a state similar to hepatoblasts (Shinozawa et al. 2021). scRNA-seq allows computation and comparison of the differentiation and developmental trajectories of iHLCs from hepatoblasts (Wesley et al. 2022). These analyses indicated that while on day 14, iHLCs aligned with hepatoblasts, their subsequent development diverged from that of hepatocytes (Wesley et al. 2022). These differences corresponded to downregulation in iHLCs of genes involved in bile acid transport, lipid metabolism, and xenobiotic metabolism (Wesley et al. 2022). Another study that characterized iHLCs and PHHs with scRNA-seq analyses found that populations of these cells formed distinct clusters in a PCA plot (Nell et al. 2022), similar to our finding for bulk RNA-seq data (Fig. 2b). Furthermore, iHLCs showed expression of selected liver and intestinal genes within the same cells. In contrast, the expression of intestinal genes was not detectable in PHHs (Nell et al. 2022).

After 48–72 h in monolayer culture, PHHs also dedifferentiate and lose their key functions (Kim and Rajagopalan 2010; Larkin et al. 2013). A CS assembly has helped PHHs remain stable for up to a 2-week period (Dunn et al. 1989; Kim and Rajagopalan 2010). However, homeostasis of hepatocytes is maintained by cell–cell signaling with other non-parenchymal cells (NPCs) of the liver (Larkin et al. 2013; Roy-Chowdhury et al. 2017; Tegge et al. 2018). We have previously showed that PHHs, when co-cultured in a 3D model with other NPCs, including liver sinusoidal endothelial cells (LSECs) and Kupffer cells, exhibit enhanced functionality including urea and albumin secretion and CYP activity (Godoy et al. 2013; Kim and Rajagopalan 2010; Larkin et al. 2013; Orbach et al. 2017, 2018). In addition, a culture with these three cell types can elicit a response to administered toxicants closer to what occurs in vivo, creating a platform for further toxicity measurements (Orbach et al. 2017, 2018).

In addition, the maturation of iHLCs could lead to their use in liver models if these cells can exhibit hepatic functions comparable to PHHs. Co-culturing iHLCs with other cell types such as LSECs, human umbilical vein endothelial cells, adipose-derived stem cells, and hepatic stellate cells for longer periods of time in a 3D matrix have shown

improved urea and albumin secretion, expression of hepatic markers, protein secretion, bile canaliculi formation, and CYP450 activity (Ardalani et al. 2019; Pettinato et al. 2019; Wang et al. 2018; Xie et al. 2021; Zhu et al. 2021). However, many of these are spheroid cultures which do not emulate liver architecture (Ardalani et al. 2019; Pettinato et al. 2019). These spheroids are also assembled with cellular ratios that do not match in vivo conditions but are optimized for in vitro culture instead (Ardalani et al. 2019; Wang et al. 2018).

Conclusions

The RNA-seq conclusions from this analysis correspond with previous studies and experimental results. Our study gives insight into the genome-wide transcriptomic analysis and the specific fold-changes of genes in differentially regulated pathways between the two cell types. Our study encourages targets of potential pathways that could improve the functionality of iHLCs. There remains tremendous potential to investigate how culturing iHLCs with other NPCs in a 3D organoid that closely recapitulates both cellular composition and architecture found in vivo can enhance their maturation and hepatic functions.

Abbreviations HFC: 7-Hydroxy-4-trifluoromethylcoumarin; MFC: 7-Methoxy-4-trifluoromethylcoumarin; APAP: Acetaminophen; AQP9: Aquaporin 9; ABC: ATP binding cassette; BMP-4: Bone morphogenic factor-4; BSA: Bovine serum albumin; CS: Collagen sandwich; CYP450: Cytochrome P450; ESCs: Embryonic stem cells; ER: Endoplasmic reticulum; EtOH: Ethanol; EDTA: Ethylenediaminetetraacetic acid; FXR: Farnesoid X receptor; FGF-2: Fibroblast growth factor-2; GSH: Glutathione; HGF: Hepatocyte growth factor; iHLCs: Hepatocyte-like cells; iPSCs: Induced pluripotent stem cells; LC_{50}: Lethal concentration 50; LSECs: Liver sinusoidal endothelial cells; mTOR: Mammalian target of rapamycin; NPCs: Non-parenchymal cells; OGDHL: Oxoglutarate dehydrogenase L; PBS: Phosphate buffered saline; PCA: Principal component analyses; PCK1: Phosphoenolpyruvate carboxykinase 1; PI3K: Phosphoinositide 3-kinase; PHHs: Primary human hepatocytes; AKT: Protein kinase B; ROS: Reactive oxygen species; SDS: Sodium dodecyl sulfate; TCPS: Tissue culture polystyrene; t-SNE: T-distributed stochastic neighbor embedding; UGT: UDP-glucuronosyltransferase

Acknowledgements Figures 1, 4c/d, and 5a/f were created using Biorender.com.

Author contribution N.G. performed statistical analysis, interpreted the data, and wrote the manuscript. L.W. performed the cellular work and assessments. K.A. performed the RNA-seq analysis and interpreted the results. Y.S. assisted with revisions and analyzing the RNA-seq data. P.N. assisted with revisions to the manuscript. T.M.M. and P.R. designed the scope of the paper, supervised, and wrote the paper.

Funding The authors gratefully acknowledge support for this work from the National Science Foundation (NSF DBI-1759858, T.M.M., K.A., and Y.S.; DBI-2233967, T.M.M. and Y.S.; NSF 2200045, T.M.M. and P.R.), Institute for Critical Technologies and Applied Science, Virginia Tech (P.R. and N.G.), and the Computational Tissue Engineering Interdisciplinary Graduate Education Program, Virginia Tech (T.M.M. and P.R.).

Availability of data and materials We will make the RNA-seq data available in the Gene Expression Omnibus upon publication. All experimental supplies were obtained from commercial vendors.

Declarations

Conflict of interest The authors declare no competing interests.

References

Akram M (2014) Citric acid cycle and role of its intermediates in metabolism. Cell Biochem Biophys 68(3):475–478. https://doi.org/10.1007/s12013-013-9750-1

Allain EP, Rouleau M, Lévesque E, Guillemette C (2020) Emerging roles for UDP-glucuronosyltransferases in drug resistance and cancer progression. Br J Cancer 122(9):1277–1287. https://doi.org/10.1038/s41416-019-0722-0

Anand U, Anand CV (1999) Connecting links between the urea cycle and the TCA cycle: a tutorial exercise. Biochemical Education 27(3):153–154. https://doi.org/10.1016/S0307-4412(99)00041-2

Ardalani H, Sengupta S, Harms V, Vickerman V, Thomson JA, Murphy WL (2019) 3-D culture and endothelial cells improve maturity of human pluripotent stem cell-derived hepatocytes. Acta Biomater 95:371–381. https://doi.org/10.1016/j.actbio.2019.07.047

Arias IM, Alter HJ, Boyer JL, Cohen DE, Shafritz DA, Thorgeirsson SS, Wolkoff AW (2009) The Liver: Biology and Pathobiology, 5th edn. Wiley, Hoboken, NJ. ISBN: 9780470723135

Barbier O, Trottier J, Kaeding J, Caron P, Verreault M (2009) Lipid-activated transcription factors control bile acid glucuronidation. Mol Cell Biochem 326(1–2):3–8. https://doi.org/10.1007/s11010-008-0001-5

Brazovskaja A, Treutlein B, Camp JG (2019) High-throughput single-cell transcriptomics on organoids. Curr Opin Biotechnol 55:167–171. https://doi.org/10.1016/j.copbio.2018.11.002

Camp JG, Sekine K, Gerber T, Loeffler-Wirth H, Binder H, Gac M, Kanton S, Kageyama J, Damm G, Seehofer D, Belicova L, Bickle M, Barsacchi R, Okuda R, Yoshizawa E, Kimura M, Ayabe H, Taniguchi H, Takebe T, Treutlein B (2017) Multilineage communication regulates human liver bud development from pluripotency. Nature 546(7659):533–538. https://doi.org/10.1038/nature22796

Chen T, Oh S, Gregory S, Shen X, Diehl AM (2020) Single-cell omics analysis reveals functional diversification of hepatocytes during liver regeneration. JCI Insight 5(22). https://doi.org/10.1172/jci.insight.141024

Chiang JYL (2013) Bile acid metabolism and signaling. Compr Physiol 3(3):1191–1212. https://doi.org/10.1002/cphy.c120023

Choudhury Y, Toh YC, Xing J, Qu Y, Poh J, Li H, Tan HS, Kanesvaran R, Yu H, Tan M-H (2017) Patient-specific hepatocyte-like cells derived from induced pluripotent stem cells model pazopanib-mediated hepatotoxicity. Sci Rep 7(1):41238. https://doi.org/10.1038/srep41238

Dao Thi VL, Wu X, Belote RL, Andreo U, Takacs CN, Fernandez JP, Vale-Silva LA, Prallet S, Decker CC, Fu RM, Qu B, Uryu K, Molina H, Saeed M, Steinmann E, Urban S, Singaraja RR, Schneider WM, Simon SM, Rice CM (2020) Stem cell-derived polarized hepatocytes. Nat Commun 11(1):1677. https://doi.org/10.1038/s41467-020-15337-2

David S, Hamilton JP (2010) Drug-induced liver injury. US Gastroenterol Hepatol Rev 6:73–80

de Cima S, Polo LM, Díez-Fernández C, Martínez AI, Cervera J, Fita I, Rubio V (2015) Structure of human carbamoyl phosphate synthetase: deciphering the on/off switch of human ureagenesis. Sci Rep 5(1):16950. https://doi.org/10.1038/srep16950

Detzel CJ, Kim Y, Rajagopalan P (2011) Engineered three-dimensional liver mimics recapitulate critical rat-specific bile acid pathways. Tissue Eng Part A 17(5–6):677–689. https://doi.org/10.1089/ten.TEA.2010.0423

Donato MT, Jiménez N, Castell JV, Gómez-Lechón MJ (2004) Fluorescence-based assays for screening nine cytochrome P450 (P450) activities in intact cells expressing individual human P450 enzymes. Drug Metab Dispos 32(7):699–706. https://doi.org/10.1124/dmd.32.7.699

Du Y, Wang J, Jia J, Song N, Xiang C, Xu J, Hou Z, Su X, Liu B, Jiang T, Zhao D, Sun Y, Shu J, Guo Q, Yin M, Sun D, Lu S, Shi Y, Deng H (2014) Human hepatocytes with drug metabolic function induced from fibroblasts by lineage reprogramming. Cell Stem Cell 14(3):394–403. https://doi.org/10.1016/j.stem.2014.01.008

Du C, Feng Y, Qiu D, Xu Y, Pang M, Cai N, Xiang AP, Zhang Q (2018) Highly efficient and expedited hepatic differentiation from human pluripotent stem cells by pure small-molecule cocktails. Stem Cell Res Ther 9(1):58. https://doi.org/10.1186/s13287-018-0794-4

Dunn JC, Yarmush ML, Koebe HG, Tompkins RG (1989) Hepatocyte function and extracellular matrix geometry: long-term culture in a sandwich configuration. FASEB J 3(2):174–177

Gao X, Liu Y (2017) A transcriptomic study suggesting human iPSC-derived hepatocytes potentially offer a better in vitro model of hepatotoxicity than most hepatoma cell lines. Cell Biol Toxicol 33(4):407–421. https://doi.org/10.1007/s10565-017-9383-z

Godoy P, Hewitt NJ, Albrecht U, Andersen ME, Ansari N, Bhattacharya S, Bode JG, Bolleyn J, Borner C, Böttger J, Braeuning A, Budinsky RA, Burkhardt B, Cameron NR, Camussi G, Cho C-S, Choi Y-J, Craig Rowlands J, Dahmen U, ... Hengstler JG (2013) Recent advances in 2D and 3D in vitro systems using primary hepatocytes, alternative hepatocyte sources and non-parenchymal liver cells and their use in investigating mechanisms of hepatotoxicity, cell signaling and ADME. Arch Toxicol 87(8):1315–1530. https://doi.org/10.1007/s00204-013-1078-5

Grant R, Hallett J, Forbes S, Hay D, Callanan A (2019) Blended electrospinning with human liver extracellular matrix for engineering new hepatic microenvironments. Sci Rep 9(1):6293. https://doi.org/10.1038/s41598-019-42627-7

Guo C, Sun L, Chen X, Zhang D (2013) Oxidative stress, mitochondrial damage and neurodegenerative diseases. Neural Regen Res 8(21):2003–2014. https://doi.org/10.3969/j.issn.1673-5374.2013.21.009

Gupta R, Schrooders Y, Hauser D, van Herwijnen M, Albrecht W, Ter Braak B, Brecklinghaus T, Castell JV, Elenschneider L, Escher S, Guye P, Hengstler JG, Ghallab A, Hansen T, Leist M, Maclennan R, Moritz W, Tolosa L, Tricot T, ... Caiment F (2021) Comparing in vitro human liver models to in vivo human liver using RNA-Seq. Arch Toxicol 95(2):573–589. https://doi.org/10.1007/s00204-020-02937-6

Guttman Y, Nudel A, Kerem Z (2019) Polymorphism in cytochrome P450 3A4 is ethnicity related. Front Genet 10:224. https://doi.org/10.3389/fgene.2019.00224

Harris MA, Clark J, Ireland A, Lomax J, Ashburner M, Foulger R, Eilbeck K, Lewis S, Marshall B, Mungall C, Richter J, Rubin GM, Blake JA, Bult C, Dolan M, Drabkin H, Eppig JT, Hill DP, Ni L, ..., White R (2004) The Gene Ontology (GO) database and informatics resource. Nucleic Acids Res 32(Database issue):D258-261. https://doi.org/10.1093/nar/gkh036

Herrero J, Muffato M, Beal K, Fitzgerald S, Gordon L, Pignatelli M, Vilella AJ, Searle SM, Amode R, Brent S, Spooner W, Kulesha E, Yates A, Flicek P (2016) Ensembl comparative genomics resources. Database (Oxford) 2016:bav096. https://doi.org/10.1093/database/bav096. Erratum in: Database (Oxford). 2016;2016. pii: baw053. https://doi.org/10.1093/database/baw053. PMID: 26896847; PMCID: PMC4761110

Jansen PL (2017) Fibroblast growth factor 19, a double-edged sword. Hepat Oncol 4(1):1–4. https://doi.org/10.2217/hep-2017-0008

Jelen S, Gena P, Lebeck J, Rojek A, Praetorius J, Frøkiaer J, Fenton RA, Nielsen S, Calamita G, Rützler M (2012) Aquaporin-9 and urea transporter-A gene deletions affect urea transmembrane passage in murine hepatocytes. Am J Physiol Gastrointest Liver Physiol 303(11):G1279-1287. https://doi.org/10.1152/ajpgi.00153.2012

Jolliffe IT (2002) Principal component analysis for special types of data. In: Jolliffe IT (ed) Principal component analysis. Springer, New York, pp 338–372. https://doi.org/10.1007/0-387-22440-8_13

Kaserman JE, Wilson AA (2017) Protocol for directed differentiation of human induced pluripotent stem cells (iPSCs) to a hepatic lineage. Methods Mol Biol 1639:151–160. https://doi.org/10.1007/978-1-4939-7163-3_15

Kim Y, Rajagopalan P (2010) 3D hepatic cultures simultaneously maintain primary hepatocyte and liver sinusoidal endothelial cell phenotypes. PLoS ONE 5(11):e15456. https://doi.org/10.1371/journal.pone.0015456

Kim Y, Larkin AL, Davis RM, Rajagopalan P (2010) The design of in vitro liver sinusoid mimics using chitosan-hyaluronic acid polyelectrolyte multilayers. Tissue Eng Part A 16(9):2731–2741. https://doi.org/10.1089/ten.tea.2009.0695

Kim D, Langmead B, Salzberg SL (2015) HISAT: a fast spliced aligner with low memory requirements. Nat Methods 12(4):357–360. https://doi.org/10.1038/nmeth.3317

Klaassen CD (2013) Casarett and Doull's toxicology: the basic science of poisons (Vol. 1236), vol 1236. McGraw-Hill, New York

Klein K, Winter S, Turpeinen M, Schwab M, Zanger UM (2010) Pathway-targeted pharmacogenomics of CYP1A2 in human liver. Front Pharmacol 1:129–129. https://doi.org/10.3389/fphar.2010.00129

Kocarek TA, Zangar RC, Novak RF (2000) Post-transcriptional regulation of rat CYP2E1 expression: role of CYP2E1 mRNA untranslated regions in control of translational efficiency and message stability. Arch Biochem Biophys 376(1):180–190. https://doi.org/10.1006/abbi.2000.1704

Kroll T, Prescher M, Smits SHJ, Schmitt L (2021) Structure and function of hepatobiliary ATP binding cassette transporters. Chem Rev 121(9):5240–5288. https://doi.org/10.1021/acs.chemrev.0c00659

Krumm J, Sekine K, Samaras P, Brazovskaja A, Breunig M, Yasui R, Kleger A, Taniguchi H, Wilhelm M, Treutlein B, Camp JG, Kuster B (2022) High temporal resolution proteome and phosphoproteome profiling of stem cell-derived hepatocyte development. Cell Rep 38(13):110604. https://doi.org/10.1016/j.celrep.2022.110604

Kuna L, Bozic I, Kizivat T, Bojanic K, Mrso M, Kralj E, Smolic R, Wu GY, Smolic M (2018) Models of drug induced liver injury (DILI) - current issues and future perspectives. Curr Drug Metab 19(10):830–838. https://doi.org/10.2174/1389200219666180523095355

Larkin AL, Rodrigues RR, Murali TM, Rajagopalan P (2013) Designing a multicellular organotypic 3D liver model with a detachable, nanoscale polymeric Space of Disse. Tissue Eng Part C Methods 19(11):875–884. https://doi.org/10.1089/ten.TEC.2012.0700

Laudadio I, Manfroid I, Achouri Y, Schmidt D, Wilson MD, Cordi S, Thorrez L, Knoops L, Jacquemin P, Schuit F, Pierreux CE, Odom DT, Peers B, Lemaigre FP (2012) A feedback loop between the liver-enriched transcription factor network and miR-122 controls hepatocyte differentiation. Gastroenterology 142(1):119–129. https://doi.org/10.1053/j.gastro.2011.09.001

Laurens van der Maaten GH (2008) Visualizing data using t-SNE. J Mach Learn Res 9(86):2579–2605

Lauschke VM, Hendriks DF, Bell CC, Andersson TB, Ingelman-Sundberg M (2016) Novel 3D culture systems for studies of human liver function and assessments of the hepatotoxicity of drugs and drug candidates. Chem Res Toxicol 29(12):1936–1955. https://doi.org/10.1021/acs.chemrestox.6b00150

Leung TM, Nieto N (2013) CYP2E1 and oxidant stress in alcoholic and non-alcoholic fatty liver disease. J Hepatol 58(2):395–398. https://doi.org/10.1016/j.jhep.2012.08.018

Liao Y, Smyth GK, Shi W (2014) featureCounts: an efficient general purpose program for assigning sequence reads to genomic features. Bioinformatics 30(7):923–930. https://doi.org/10.1093/bioinformatics/btt656

Lindley C, Hamilton G, McCune JS, Faucette S, Shord SS, Hawke RL, Wang H, Gilbert D, Jolley S, Yan B, LeCluyse EL (2002) The effect of cyclophosphamide with and without dexamethasone on cytochrome P450 3A4 and 2B6 in human hepatocytes. Drug Metab Dispos 30(7):814–822. https://doi.org/10.1124/dmd.30.7.814

Liu L-G, Yan H, Yao P, Zhang W, Zou L-J, Song F-F, Li K, Sun X-F (2005) CYP2E1-dependent hepatotoxicity and oxidative damage after ethanol administration in human primary hepatocytes. World J Gastroenterol 11(29):4530–4535. https://doi.org/10.3748/wjg.v11.i29.4530

Liu D, Yu Q, Li Z, Zhang L, Hu M, Wang C, Liu Z (2021) UGT1A1 dysfunction increases liver burden and aggravates hepatocyte damage caused by long-term bilirubin metabolism disorder. Biochem Pharmacol 190:114592. https://doi.org/10.1016/j.bcp.2021.114592

Love MI, Huber W, Anders S (2014) Moderated estimation of fold change and dispersion for RNA-seq data with DESeq2. Genome Biol 15(12):550. https://doi.org/10.1186/s13059-014-0550-8

Lu Y, Cederbaum AI (2008) CYP2E1 and oxidative liver injury by alcohol. Free Radical Biol Med 44(5):723–738. https://doi.org/10.1016/j.freeradbiomed.2007.11.004

Madhunapantula SV, Mosca PJ, Robertson GP (2011) The Akt signaling pathway: an emerging therapeutic target in malignant melanoma. Cancer Biol Ther 12(12):1032–1049. https://doi.org/10.4161/cbt.12.12.18442

Mallanna SK, Duncan SA (2013) Differentiation of hepatocytes from pluripotent stem cells. Curr Protoc Stem Cell Biol 26:1g.4.1-1g.4.13. https://doi.org/10.1002/9780470151808.sc01g04s26

Manley S, Ding W (2015) Role of farnesoid X receptor and bile acids in alcoholic liver disease. Acta Pharm Sin B 5(2):158–167. https://doi.org/10.1016/j.apsb.2014.12.011

Marinelli RA, Lehmann GL, Soria LR, Marchissio MJ (2011) Hepatocyte aquaporins in bile formation and cholestasis. Front Biosci (landmark Ed) 16(7):2642–2652. https://doi.org/10.2741/3877

Maruo Y, Iwai M, Mori A, Sato H, Takeuchi Y (2005) Polymorphism of UDP-glucuronosyltransferase and drug metabolism. Curr Drug Metab 6(2):91–99. https://doi.org/10.2174/1389200053586064

Montal ED, Bhalla K, Dewi RE, Ruiz CF, Haley JA, Ropell AE, Gordon C, Haley JD, Girnun GD (2019) Inhibition of phosphoenolpyruvate carboxykinase blocks lactate utilization and impairs tumor growth in colorectal cancer. Cancer Metab 7(1):8. https://doi.org/10.1186/s40170-019-0199-6

Mora C, Serzanti M, Consiglio A, Memo M, Dell'Era P (2017) Clinical potentials of human pluripotent stem cells. Cell Biol Toxicol 33(4):351–360. https://doi.org/10.1007/s10565-017-9384-y

Nakamori D, Akamine H, Takayama K, Sakurai F, Mizuguchi H (2017) Direct conversion of human fibroblasts into hepatocyte-like cells by ATF5, PROX1, FOXA2, FOXA3, and HNF4A transduction. Sci Rep 7(1):16675. https://doi.org/10.1038/s41598-017-16856-7

Nell P, Kattler K, Feuerborn D, Hellwig B, Rieck A, Salhab A, Lepikhov K, Gasparoni G, Thomitzek A, Belgasmi K, Blüthgen N, Morkel M, Küppers-Munther B, Godoy P, Hay DC, Cadenas C, Marchan R, Vartak N, Edlund K, Hengstler JG (2022) Identification of an FXR-modulated liver-intestine hybrid state in iPSC-derived hepatocyte-like cells. J Hepatol 77(5):1386–1398. https://doi.org/10.1016/j.jhep.2022.07.009

Neve EP, Ingelman-Sundberg M (2000) Molecular basis for the transport of cytochrome P450 2E1 to the plasma membrane. J Biol Chem 275(22):17130–17135. https://doi.org/10.1074/jbc.M000957200

Novak RF, Woodcroft KJ (2000) The alcohol-inducible form of cytochrome P450 (CYP 2E1): role in toxicology and regulation of expression. Arch Pharm Res 23(4):267–282. https://doi.org/10.1007/bf02975435

Orbach SM, Cassin ME, Ehrich MF, Rajagopalan P (2017) Investigating acetaminophen hepatotoxicity in multi-cellular organotypic liver models. In Vitro Toxicol 42:10–20. https://doi.org/10.1016/j.tiv.2017.03.008

Orbach SM, Ehrich MF, Rajagopalan P (2018) High-throughput toxicity testing of chemicals and mixtures in organotypic multi-cellular cultures of primary human hepatic cells. In Vitro Toxicol 51:83–94. https://doi.org/10.1016/j.tiv.2018.05.006

Orge ID, Gadd VL, Barouh JL, Rossi EA, Carvalho RH, Smith I, Allahdadi KJ, Paredes BD, Silva DN, Damasceno PKF, Sampaio GL, Forbes SJ, Soares MBP, Souza BS, d. F. (2020) Phenotype instability of hepatocyte-like cells produced by direct reprogramming of mesenchymal stromal cells. Stem Cell Res Ther 11(1):154. https://doi.org/10.1186/s13287-020-01665-z

Overeem AW, Klappe K, Parisi S, Klöters-Planchy P, Mataković L, du Teil Espina M, Drouin CA, Weiss KH, van, I. S. C. D. (2019) Pluripotent stem cell-derived bile canaliculi-forming hepatocytes to study genetic liver diseases involving hepatocyte polarity. J Hepatol 71(2):344–356. https://doi.org/10.1016/j.jhep.2019.03.031

Perugorria MJ, Olaizola P, Labiano I, Esparza-Baquer A, Marzioni M, Marin JJG, Bujanda L, Banales JM (2019) Wnt–β-catenin signalling in liver development, health and disease. Nat Rev Gastroenterol Hepatol 16(2):121–136. https://doi.org/10.1038/s41575-018-0075-9

Pettinato G, Lehoux S, Ramanathan R, Salem MM, He L-X, Muse O, Flaumenhaft R, Thompson MT, Rouse EA, Cummings RD, Wen X, Fisher RA (2019) Generation of fully functional hepatocyte-like organoids from human induced pluripotent stem cells mixed with endothelial cells. Sci Rep 9(1):8920. https://doi.org/10.1038/s41598-019-45514-3

Preissner SC, Hoffmann MF, Preissner R, Dunkel M, Gewiess A, Preissner S (2013) Polymorphic cytochrome P450 enzymes (CYPs) and their role in personalized therapy. PLoS ONE 8(12):e82562. https://doi.org/10.1371/journal.pone.0082562

Ramli MNB, Lim YS, Koe CT, Demircioglu D, Tng W, Gonzales KAU, Tan CP, Szczerbinska I, Liang H, Soe EL, Lu Z, Ariyachet C, Yu KM, Koh SH, Yaw LP, Jumat NHB, Lim JSY, Wright G, Shabbir A, ... Chan Y-S (2020) Human pluripotent stem cell-derived organoids as models of liver disease. Gastroenterology 159(4):1471–1486. https://doi.org/10.1053/j.gastro.2020.06.010

Rowe RG, Daley GQ (2019) Induced pluripotent stem cells in disease modelling and drug discovery. Nat Rev Genet 20(7):377–388. https://doi.org/10.1038/s41576-019-0100-z

Rowland A, Miners JO, Mackenzie PI (2013) The UDP-glucuronosyltransferases: their role in drug metabolism and detoxification. Int J Biochem Cell Biology 45(6):1121–1132. https://doi.org/10.1016/j.biocel.2013.02.019

Roy-Chowdhury N, Wang X, Guha C, Roy-Chowdhury J (2017) Hepatocyte-like cells derived from induced pluripotent stem cells. Hepatol Int 11(1):54–69. https://doi.org/10.1007/s12072-016-9757-y

Rui L (2014) Energy metabolism in the liver. Compr Physiol 4(1):177–197. https://doi.org/10.1002/cphy.c130024

Sauer V, Roy-Chowdhury N, Guha C, Roy-Chowdhury J (2014) Induced pluripotent stem cells as a source of hepatocytes. Curr Pathobiol Rep 2(1):11–20. https://doi.org/10.1007/s40139-013-0039-2

Shambaugh GE 3rd (1977) Urea biosynthesis I. The urea cycle and relationships to the citric acid cycle. Am J Clin Nutr 30(12):2083–2087. https://doi.org/10.1093/ajcn/30.12.2083

Shi Y, Inoue H, Wu JC, Yamanaka S (2017) Induced pluripotent stem cell technology: a decade of progress. Nat Rev Drug Discovery 16(2):115–130. https://doi.org/10.1038/nrd.2016.245

Shinozawa T, Kimura M, Cai Y, Saiki N, Yoneyama Y, Ouchi R, Koike H, Maezawa M, Zhang RR, Dunn A, Ferguson A, Togo S, Lewis K, Thompson WL, Asai A, Takebe T (2021) High-fidelity drug-induced liver injury screen using human pluripotent stem cell-derived organoids. Gastroenterology 160(3):831-846.e810. https://doi.org/10.1053/j.gastro.2020.10.002

Si-Tayeb K, Noto FK, Nagaoka M, Li J, Battle MA, Duris C, North PE, Dalton S, Duncan SA (2010) Highly efficient generation of human hepatocyte-like cells from induced pluripotent stem cells. Hepatology 51(1):297–305. https://doi.org/10.1002/hep.23354

Sivandzade F, Bhalerao A, Cucullo L (2019) Analysis of the mitochondrial membrane potential using the cationic JC-1 dye as a sensitive fluorescent probe. Bio Protoc 9(1). https://doi.org/10.21769/BioProtoc.3128

Sjogren A-KM, Liljevald M, Glinghammar B, Sagemark J, Li X-Q, Jonebring A, Cotgreave I, Brolén G, Andersson TB (2014) Critical differences in toxicity mechanisms in induced pluripotent stem cell-derived hepatocytes, hepatic cell lines and primary hepatocytes. Arch Toxicol 88(7):1427–1437. https://doi.org/10.1007/s00204-014-1265-z

Song Z, Cai J, Liu Y, Zhao D, Yong J, Duo S, Song X, Guo Y, Zhao Y, Qin H, Yin X, Wu C, Che J, Lu S, Ding M, Deng H (2009) Efficient generation of hepatocyte-like cells from human induced pluripotent stem cells. Cell Res 19(11):1233–1242. https://doi.org/10.1038/cr.2009.107

Stark R, Pasquel F, Turcu A, Pongratz RL, Roden M, Cline GW, Shulman GI, Kibbey RG (2009) Phosphoenolpyruvate cycling via mitochondrial phosphoenolpyruvate carboxykinase links anaplerosis and mitochondrial GTP with insulin secretion. J Biol Chem 284(39):26578–26590. https://doi.org/10.1074/jbc.M109.011775

Takahashi K, Yamanaka S (2006) Induction of pluripotent stem cells from mouse embryonic and adult fibroblast cultures by defined factors. Cell 126(4):663–676. https://doi.org/10.1016/j.cell.2006.07.024

Takebe T, Sekine K, Enomura M, Koike H, Kimura M, Ogaeri T, Zhang R-R, Ueno Y, Zheng Y-W, Koike N, Aoyama S, Adachi Y, Taniguchi H (2013) Vascularized and functional human liver from an iPSC-derived organ bud transplant. Nature 499(7459):481–484. https://doi.org/10.1038/nature12271

Tegge AN, Rodrigues RR, Larkin AL, Vu L, Murali TM, Rajagopalan P (2018) Transcriptomic analysis of hepatic cells in multicellular organotypic liver models. Sci Rep 8(1):11306. https://doi.org/10.1038/s41598-018-29455-x

Tzanakakis ES, Hansen LK, Hu WS (2001) The role of actin filaments and microtubules in hepatocyte spheroid self-assembly. Cell Motil Cytoskeleton 48(3):175–189. https://doi.org/10.1002/1097-0169(200103)48:3%3c175::Aid-cm1007%3e3.0.Co;2-2

Viiri LE, Rantapero T, Kiamehr M, Alexanova A, Oittinen M, Viiri K, Niskanen H, Nykter M, Kaikkonen MU, Aalto-Setälä K (2019) Extensive reprogramming of the nascent transcriptome during iPSC to hepatocyte differentiation. Sci Rep 9(1):3562. https://doi.org/10.1038/s41598-019-39215-0

Wang Z, Gerstein M, Snyder M (2009) RNA-Seq: a revolutionary tool for transcriptomics. Nat Rev Genet 10(1):57–63. https://doi.org/10.1038/nrg2484

Wang J, Zhao P, Wan Z, Jin X, Cheng Y, Yan T, Qing S, Ding N, Xin S (2016) Differentiation of human foreskin fibroblast-derived induced pluripotent stem cells into hepatocyte-like cells. Cell Biochem Funct 34(7):475–482. https://doi.org/10.1002/cbf.3210

Wang G, Zheng Y, Wang Y, Cai Z, Liao N, Liu J, Zhang W (2018) Co-culture system of hepatocytes and endothelial cells: two in vitro approaches for enhancing liver-specific functions of hepatocytes. Cytotechnology 70(4):1279–1290. https://doi.org/10.1007/s10616-018-0219-3

Wang Z, Dong C (2019) Gluconeogenesis in cancer: function and regulation of PEPCK, FBPase, and G6Pase. Trends in Cancer 5(1):30–45. https://doi.org/10.1016/j.trecan.2018.11.003

Wesley BT, Ross ADB, Muraro D, Miao Z, Saxton S, Tomaz RA, Morell CM, Ridley K, Zacharis ED, Petrus-Reurer S, Kraiczy J, Mahbubani KT, Brown S, Garcia-Bernardo J, Alsinet C, Gaffney D, Horsfall D, Tysoe OC, Botting RA, ... Vallier L (2022) Single-cell atlas of human liver development reveals pathways directing hepatic cell fates. Nat Cell Biol 24(10):1487–1498. https://doi.org/10.1038/s41556-022-00989-7

Wickham H (2011) ggplot2. Wiley Interdisciplinary Reviews: Computational Statistics 3(2):180–185

Wills LR, Rajagopalan P (2020) Advances in human induced pluripotent stem cell-derived hepatocytes for use in toxicity testing. Ann Biomed Eng 48(3):1045–1057. https://doi.org/10.1007/s10439-019-02331-z

Xiang J, Wang K, Tang N (2023) PCK1 dysregulation in cancer: metabolic reprogramming, oncogenic activation, and therapeutic opportunities. Genes Dis 10(1):101–112. https://doi.org/10.1016/j.gendis.2022.02.010

Xie Y, Yao J, Jin W, Ren L, Li X (2021) Induction and maturation of hepatocyte-like cells in vitro: focus on technological advances and challenges [Review]. Front Cell Dev Biol 9. https://doi.org/10.3389/fcell.2021.765980

Xu Z, He X, Shi X, Xia Y, Liu X, Wu H, Li P, Zhang H, Yin W, Du X, Li L, Li Y (2018) Analysis of differentially expressed genes among human hair follicle–derived iPSCs, induced hepatocyte-like cells, and primary hepatocytes. Stem Cell Res Ther 9(1):211. https://doi.org/10.1186/s13287-018-0940-z

Yu G, Wang LG, Han Y, He QY (2012) clusterProfiler: an R package for comparing biological themes among gene clusters. OMICS 16(5):284–287. https://doi.org/10.1089/omi.2011.0118

Yu S, Meng S, Xiang M, Ma H (2021) Phosphoenolpyruvate carboxykinase in cell metabolism: roles and mechanisms beyond gluconeogenesis. Mol Metab 53:101257. https://doi.org/10.1016/j.molmet.2021.101257

Zanger UM, Schwab M (2013) Cytochrome P450 enzymes in drug metabolism: regulation of gene expression, enzyme activities, and impact of genetic variation. Pharmacol Ther 138(1):103–141. https://doi.org/10.1016/j.pharmthera.2012.12.007

Zeilinger K, Freyer N, Damm G, Seehofer D, Knöspel F (2016) Cell sources for in vitro human liver cell culture models. Exp Biol Med (maywood) 241(15):1684–1698. https://doi.org/10.1177/1535370216657448

Zhang X, Jonassen I (2020) RASflow: an RNA-Seq analysis workflow with Snakemake. BMC Bioinformatics 21(1):110. https://doi.org/10.1186/s12859-020-3433-x

Zhang W, Li W, Liu B, Wang P, Li W, Zhang H (2012) Efficient generation of functional hepatocyte-like cells from human fetal hepatic progenitor cells in vitro. J Cell Physiol 227(5):2051–2058. https://doi.org/10.1002/jcp.22934

Zhou SF, Xue CC, Yu XQ, Li C, Wang G (2007) Clinically important drug interactions potentially involving mechanism-based inhibition of cytochrome P450 3A4 and the role of therapeutic drug monitoring. Ther Drug Monit 29(6):687–710. https://doi.org/10.1097/FTD.0b013e31815c16f5

Zhu X, Zhang B, He Y, Bao J (2021) Liver organoids: formation strategies and biomedical applications. Tissue Eng Regen Med 18(4):573–585. https://doi.org/10.1007/s13770-021-00357-w